

Measurements of 0.2 to 20 GeV/n cosmic-ray proton and helium spectra from 1997 through 2002 with the BESS spectrometer

Y. Shikaze^{a,1}, S. Haino^{b,*}, K. Abe^{a,2}, H. Fukue^c, T. Hams^d,
 K. C. Kim^e, Y. Makida^b, S. Matsuda^b, J. W. Mitchell^d,
 A. A. Moiseev^d, J. Nishimura^f, M. Nozaki^b, S. Orito^{f,3},
 J. F. Ormes^{d,4}, T. Sanuki^f, M. Sasaki^d, E. S. Seo^e,
 R. E. Streitmatter^d, J. Suzuki^b, K. Tanaka^b, T. Yamagami^c,
 A. Yamamoto^b, T. Yoshida^c, K. Yoshimura^b

^a*Kobe University, Kobe, Hyogo 657-8501, Japan*

^b*High Energy Accelerator Research Organization (KEK), Tsukuba, Ibaraki 305-0801, Japan*

^c*Institute of Space and Astronautical Science, Japan Aerospace Exploration Agency (ISAS/JAXA), Sagamihara, Kanagawa 229-8510, Japan*

^d*National Aeronautics and Space Administration, Goddard Space Flight Center (NASA/GSFC), Greenbelt, MD 20771, USA*

^e*University of Maryland, College Park, MD 20742, USA*

^f*The University of Tokyo, Bunkyo, Tokyo 113-0033 Japan*

Abstract

We measured low energy cosmic-ray proton and helium spectra in the kinetic energy range 0.215 – 21.5 GeV/n at different solar activities during a period from 1997 to 2002. The observations were carried out with the BESS spectrometer launched on a balloon at Lynn Lake, Canada. A calculation for the correction of secondary particle backgrounds from the overlying atmosphere was improved by using the measured spectra at small atmospheric depths ranging from 5 through 37 g/cm². The spectra at the top of atmosphere were determined within overall uncertainties of 12% for protons and 18% for helium nuclei, including statistical and systematic errors.

Key words: cosmic-ray proton, cosmic-ray helium, atmospheric proton, solar modulation, superconducting spectrometer

PACS: 95.85.Ry, 96.40.De, 96.40.Kk, 29.30.Aj

1 Introduction

Cosmic rays, charged particles from space, enter the atmosphere at a rate of several thousands per square meter per second. Among the cosmic-ray particles, protons and helium nuclei are dominant components. Thus the energy spectra and absolute fluxes of these particles constitute fundamental data for studying cosmic-ray phenomena. The interstellar spectra carry important information on the origins and propagation of cosmic rays in the Galaxy. At low energies, observable spectra in the heliosphere are deformed in a manner that depends on the solar activity.

Cosmic-ray spectra observed at balloon altitudes suffer from a large background of secondary particles produced inside the residual atmosphere. Therefore, in order to obtain the interstellar spectra and to understand the solar modulation, precise estimation of the atmospheric effects is important. The secondary components of protons are estimated by solving coupled transport equations (see for example Papini *et al.* [1]) or by performing Monte Carlo simulations assuming elementary nuclear interaction models between cosmic rays and atmospheric nuclei. The estimated secondary components can be checked and modified by comparing them with observed spectra at various atmospheric depths. For particles below the geomagnetic cut-off rigidity, atmospheric cosmic-ray spectra consist of purely secondary particles, and therefore, cosmic-ray measurements at high geomagnetic cut-off rigidity at various altitudes are useful to improve the accuracy of the estimation of the atmospheric secondary particle contribution.

We report here 0.215 to 21.5 GeV/n cosmic-ray proton and helium spectra measured by the BESS spectrometer for five balloon flights from Lynn Lake, Canada during the period 1997 through 2002. We also report on a realistic estimation of the atmospheric proton spectrum, which was tuned to be consistent with the proton spectra observed by the BESS spectrometer at small atmospheric depths.

* Corresponding author.

Email address: haino@post.kek.jp (S. Haino).

¹ Present address: Japan Atomic Energy Research Institute, Tokai-mura, Naka-gun, Ibaraki 319-1195, Japan

² Present address: ICRR, The University of Tokyo, Kashiwa, Chiba 227-8582, Japan

³ deceased.

⁴ Present address: University of Denver, Denver, Colorado, 80208, USA

2 Spectrometer

The detector for Balloon-borne Experiment with a Superconducting Spectrometer (BESS) is a high-resolution rigidity ($R \equiv P_e/Ze$) spectrometer with a large geometrical acceptance. It was designed [2,3] and developed [4,5,6,7] as an omni-purpose spectrometer to perform precise flux measurements of various components of cosmic rays [8,9,10,11,12], as well as highly sensitive searches for rare cosmic rays [13,14,15,16,17,18]. Fig. 1 shows a schematic cross-sectional view of the spectrometer in its 1997 configuration. The large acceptance is realized with a cylindrical structure and makes it possible to perform precise flux measurements with high statistics and small systematic errors.

The spectrometer consists of a superconducting solenoid coil [3], a JET type drift chamber (JET), two inner drift chambers (IDCs), Time-of-Flight (TOF) plastic scintillation hodoscopes [6], and an aerogel Čerenkov counter [7]. A uniform magnetic field of 1 Tesla is produced by the thin superconducting coil which allows particles to pass through with small interaction probability. The magnetic field variation is less than 2.5% along a typical trajectory. The magnetic field region is filled with the central tracking detectors. Tracking of incident charged particles is performed by a circular fitting [19] of up to 28 hit points, each with a spatial resolution less than $200 \mu\text{m}$, resulting in a rigidity resolution of 0.5% at 1 GV. The continuous, redundant, and three-dimensional tracking makes it possible to recognize background events with interaction or scattering. The upper and lower TOF counters measure the velocity (β) with $1/\beta$ resolution of 1.4%, and provide two independent ionization energy loss (dE/dx) measurements in the scintillators. Particle identification by mass is performed with these measurements (R , β and dE/dx). Furthermore a threshold-type Čerenkov counter with a silica-aerogel radiator is installed below the upper TOF hodoscope. The radiator, with a refractive index of 1.03 in 1997, and 1.02 in 1998 and later, was selected to veto e^-/μ^- backgrounds for antiprotons up to 3.6 GeV in 1997, and 4.2 GeV in 1998 and later [7]. In the 2002 balloon-flight experiment, the observation was made with an upgraded detector developed for precise measurement of high energy particles up to 500 GeV [10,20].

The data acquisition sequence is initiated by a first-level TOF trigger which is generated by a coincidence of signals in the upper and lower TOF hodoscopes with a threshold of more than 1/3 of the pulse charge for minimum ionizing particles. The trigger efficiency was evaluated to be $99.4 \pm 0.2\%$ with a secondary proton beam at the KEK 12 GeV proton synchrotron [21]. The second-level trigger, which utilizes the hit patterns of the scintillator hodoscopes and the IDC for the rough rigidity determination, selects negatively charged particles preferentially to improve the statistics for the antiproton flux

measurement [16]. To build an unbiased trigger sample, one of every 60 (30 in 2000 and 10 in 2002) events is recorded. In 1997, 1998 and 1999, another threshold level in the TOF trigger was set to be at 2.5 times higher pulse than that from minimum ionizing particles and one of every 25 events was recorded to improve statistics of helium events. To improve statistics during balloon-ascending periods in 1999 and 2000, we prepared a “low-energy proton trigger” which is generated by an on-board computer with a sampling rate of 1/2 to select particles with rigidity calculated to be lower than a threshold. In the offline analysis, the “low-energy proton trigger” events are used to determine proton flux below 1.0 GeV during the ascent.

In addition, an auxiliary trigger is generated by a signal from the Čerenkov counter to record particles above threshold energy with sampling rates of 1/1 in 1998, 2000 and 2002, and 1/2 (1/1, 1/3, 1/4 during some periods) in 1999. This trigger improves the statistics for high energy particles. The efficiency of the Čerenkov trigger is evaluated as the ratio of the Čerenkov-triggered events among the unbiased trigger sample. It is higher than 90% for relativistic particles ($\beta \rightarrow 1$). For the flux determination, the Čerenkov-triggered events are utilized above 6.31 GeV (10.0 GeV in 2002) for protons and 3.98 GeV/n (5.41 GeV/n in 2002) for helium nuclei. Below these energies, the TOF-triggered events are used.

3 Data Analysis

3.1 *Balloon flight observations*

We carried out balloon flights to measure cosmic-ray spectra with the BESS spectrometer at Lynn Lake, Manitoba, Canada ($56^{\circ}5'N$, $101^{\circ}3'W$), where the geomagnetic vertical cut-off rigidity is low, approximately 0.4 GV. The balloons reached a level float altitude of 37 km. The residual atmosphere above the spectrometer was typically around 5 g/cm^2 . We also collected data during ascent in 1999, 2000 and 2002. A summary of the BESS balloon flights is listed in Table 1.

We report here primary proton and helium spectra measured at Lynn Lake in 1997, 1998, 1999, 2000 and 2002. For a precise estimation of atmospheric secondary particle contributions, proton fluxes measured during the ascent period in 1999 and 2000, and during a slow descent period in 2001 were also studied. A detailed analysis of secondary particles observed at Ft. Sumner, New Mexico, USA, where the vertical cut off rigidity is 4.2 GV, in 2001 is reported in Ref. [9].

During the period from 1997 to 2002, solar activity changed from the minimum to post-maximum as identified with sunspot number and neutron monitor data [22] as shown in Fig. 2. The magnetic field polarity also reversed during this period.

3.2 Data reduction

The procedure of data analysis and derivation of the flux was almost the same as that of the previous balloon flight data [8,9,10,11,12], except for the correction of atmospheric effects.

We selected data sets which were taken with a stable condition of the spectrometer and flight altitude. The live data-taking time of the selected data sets were 29531 sec, 25901 sec, 31890 sec, 41053 sec, and 28866 sec, in 1997, 1998, 1999, 2000, and 2002, respectively. Among the selected data sets, we first selected “non-interacted” events, i.e., those associated with particles passing through the detector without interaction. The non-interacted event was defined as an event which has only one isolated track, one or two hit-counters in each layer of the TOF hodoscopes, and proper dE/dx inside the upper TOF counters. In order to estimate efficiency of the non-interacted event selection, a Monte Carlo simulation with Geant3 [23] was performed. The probability that each particle was identified as a non-interacted event was evaluated by applying the same selection criteria to the Monte Carlo events as that applied to the observed data. The resultant efficiencies of non-interacted event selection at 0.3, 1.0 and 10 GeV/n were $82.7 \pm 0.9\%$, $83.2 \pm 0.9\%$ and $76.5 \pm 1.1\%$, respectively, for protons, and $78.2 \pm 1.6\%$, $72.2 \pm 1.6\%$ and $66.4 \pm 0.8\%$, respectively, for helium nuclei. The systematic error was estimated by comparing the hit number distribution of the TOF counters. The systematic error for protons below 1 GeV was directly determined by test of the detector using an accelerator proton beam [21]. It was 2% and 3%, below and above 1 GeV/n, respectively.

The selected non-interacted events were required to pass through the fiducial volume defined by the central region of the JET chamber, TOF counters and the aerogel radiator. In the analysis of ascent data, the zenith angle (θ) of incident particles was limited within $\cos \theta > 0.95$ to obtain nearly vertical flux. In order to check the track reconstruction efficiency inside the tracking system, the recorded events were scanned randomly, and the track reconstruction efficiency was evaluated to be $99.5 \pm 0.2\%$. It was also confirmed that the rare interacted events with more than one track are fully eliminated by the non-interacted event selection.

3.3 Particle identification

For the non-interacted events fully contained in the fiducial region, particle identification was performed as follows. The charge of the particle is identified by the ionization loss measurement. Both dE/dx signals from the upper and lower TOF scintillators were required to be proton-like. Then, particles with proton mass were selected by a $1/\beta$ -band cut. The selection of protons with the dE/dx -band cut and $1/\beta$ -band cut are shown on top and bottom in Fig. 3, respectively. Since at fixed rigidity the $1/\beta$ distribution is well described by Gaussian distribution and a half-width of the $1/\beta$ selection band was set at 3.89σ , the selection efficiency was very close to unity (99.99% for a pure Gaussian distribution). Particle identification for helium nuclei was performed in the same way. However, ^3He nuclei were included in $1/\beta$ -band cut and were counted as helium-like events. In conformity with previous experiments, all the helium-like events were treated as ^4He nuclei in the analysis such as the reconstruction from rigidity to kinetic energy, and the efficiency estimation with the Monte Carlo simulation.

3.4 Quality cut

In order to maintain the quality of the rigidity measurement, a track quality cut was applied to the track fitting parameters for high energy particles above $10\text{ GeV}/n$. A TOF quality cut was also applied to confirm consistency between the hit position inside the TOF scintillator and the extrapolated track from the JET chamber.

3.5 Contamination estimation

3.5.1 Protons

Protons were clearly identified below 1.7 GV by the mass selection as shown in Fig. 3. Above 1.7 GV, however, light particles such as positrons and muons contaminate the $1/\beta$ -band for the protons, and above 4 GV deuterons (D 's) start to contaminate it. According to a Monte Carlo simulation of atmospheric cosmic rays [24], the flux ratio of $(e^+ + \mu^+)/p$ is smaller than a few percent above 1.7 GV and decreasing with higher energy at balloon altitude. The observed D/p ratio was 2% at 3 GV by counting the number of events in each $1/\beta$ -band cut. The ratio at higher energy is expected to decrease [25] due to the decrease of escape path lengths of primary cosmic rays in the Galaxy [26]. The amount of those contaminations was as small as the statistic errors of the observed proton flux and no subtraction was made.

3.5.2 Helium nuclei

Helium nuclei were clearly identified by using both upper and lower TOF dE/dx selections. Since the $1/\beta$ -band cut includes both ^3He and ^4He , the helium flux obtained includes both ^3He and ^4He . In conformity with previous experiments, all doubly charged particles were analyzed as ^4He .

3.6 Corrections to the flux obtained at TOI

The numbers of protons and helium nuclei passing through the BESS spectrometer during the observation were obtained after correcting the detection efficiency. Then absolute flux at the top of the instrument (TOI) was obtained by taking account of energy loss inside the detector, live time, and the geometrical acceptance. The energy of each particle at TOI was calculated by summing up the ionization energy losses inside the instrument by tracing back the event trajectory. The total live time of data-taking was measured precisely by counting 1 MHz clock pulses with a scaler system gated by a “ready” status that controls the first level trigger. The geometrical acceptance was calculated by using the simulation technique [27]. In the high rigidity region where the bending of the track by the magnetic field is small, the geometrical acceptance for protons and helium nuclei is $0.160 \text{ m}^2\text{sr}$ without any limit for the zenith angle for the data at the float altitude, while it is $0.055 \text{ m}^2\text{sr}$ by limiting the zenith angle as $\cos\theta > 0.95$ for the data during the ascent period. The simple cylindrical shape and the uniform magnetic field facilitate the determination of precise geometrical acceptance. The error arising from uncertainty of the detector alignment was estimated to be 1%.

4 Corrections of atmospheric secondary particles

The flux at TOI is measured under the residual atmosphere of about 5 g/cm^2 , and consists of a primary component surviving without any nuclear interactions with air, and of a secondary component produced inside the overlying atmosphere. In order to obtain the flux at the top of the atmosphere (TOA), the secondary component must be estimated and subtracted. The secondary to primary flux ratio for protons at 0.2 GeV is as high as 1.0 and 0.3 during solar maximum and solar minimum, respectively, and the ratio decreases down to less than 3% above 10 GeV. Therefore the precise estimation of the secondary component is essentially important to obtain low energy proton flux at TOA. In this work we have tuned the estimation of atmospheric protons by using the observed data at balloon altitude as described below. For helium nuclei, the secondary to primary flux ratio is less than 5% and we used basically the

same estimation as our previous works [8,10].

The proton spectrum inside the atmosphere can be estimated by solving simultaneous transport equations following Papini *et al.* [1]. Fig. 4 shows the comparison between the observed and estimated proton spectra at several atmospheric depths observed during an ascent period at Lynn Lake in 2000, and during a descent period at Ft. Sumner, New Mexico, in 2001 [9]. Fig. 5 shows the same comparison but as a function of atmospheric depth. At Lynn Lake, the observed spectra contain both primary and secondary components, but at Ft. Sumner, the spectra below the geomagnetic cut-off energy of 3.4 GeV should be composed of purely secondary components. The dashed lines in Figs. 4 and 5 show the estimated spectra assuming the same production spectrum of atmospheric secondary protons as Papini *et al.* [1]. At all the observed atmospheric depths, the estimated spectra are much less than the observed data.

In the energy region between 0.1 and a few GeV, the dominant source of the atmospheric secondary protons is recoil protons produced by interactions between primary cosmic rays and air nuclei. We modified the energy spectrum of the recoil proton production in an iterative procedure to reproduce the observed proton spectra at several atmospheric depths between 5 and 37 g/cm². The modified production spectrum was consistent with the original work by Papini *et al.* below 0.2 GeV as shown in Fig. 6. The solid lines in Figs. 4 and 5 show the estimated spectra after the modification. The agreement between the estimation and the observation was significantly improved. We also confirmed the agreement between the estimated and observed proton flux during an ascent period in 1999. The relative contribution of the secondary component is smaller in 1999 than in 2000, which was during the solar maximum period. The modified estimation can reproduce observed data irrespective of the residual atmospheric depth or sites (Ft. Sumner and Lynn Lake).

In order to obtain the flux at the top of the atmosphere (TOA), secondary proton production and interaction loss of primary particles inside the atmosphere were estimated by solving simultaneous transport equations with the modified production spectrum. The systematic error of the atmospheric correction for proton is estimated as 12.7%, which is composed of the uncertainty of residual air depth (9.0%) and the cross section of primary cosmic rays with air nuclei (8.9%). The systematic error on the resultant proton flux is estimated by multiplying the atmospheric correction factor as 3.7% and 7.6% in 1997 and 2000, respectively, at 0.2 GeV. The systematic error becomes smaller for higher energy and is 1.2% and 1.6% in 1997 and 2000, respectively, at 1 GeV. The systematic error of atmospheric correction is as small as 1% for helium flux since the correction factor is less than 5%.

5 Results and Discussions

5.1 Proton and Helium spectra at the top of atmosphere (TOA)

We obtained proton and helium spectra at the top of atmosphere during periods of various solar activity from 1997 to 2002 as shown in Fig. 7. The numerical data are summarized in Tables 2 and 3. The overall uncertainties of the proton spectrum including statistical and systematic errors are 7.8% and 12.3% in 1997 and 2000, respectively, at 0.2 GeV, and 7.5% and 6.2% in 1997 and 2000, respectively, at 20 GeV. The overall uncertainties of the helium spectrum are 6.3% and 10.3% in 1997 and 2000, respectively, at 0.2 GeV/n, and 18.2% and 7.7% in 1997 and 2000, respectively, at 20 GeV/n. The difference of the uncertainties at 0.2 GeV/n is due to the difference of the solar activity. The large uncertainties of helium spectrum at 20 GeV/n in 1997 are due to the limited statistics. As described in Section 2, the Čerenkov-trigger was introduced from 1998 and the statistics were improved.

The proton spectra at small atmospheric depths measured during the ascent period in 1999 and 2000 are summarized in Tables 4 and 5 and in Tables 6 and 7, respectively. These data combined with the descent data in 2001 [9] were used to confirm our atmospheric corrections.

A large solar modulation effect was found both in the proton and helium spectra in 2000 as a sudden decrease. On the other hand, proton and helium flux in 2002 slightly increased from those in 2000. We observed that the change in the flux variation between 2000 and 2002 was smaller than that between 1999 and 2000 around a period of the solar magnetic field reversal.

Since we have used an improved method for making the atmospheric corrections, this analysis is improved and should replace that done in our previous papers BESS-1998 [8], -1999 and -2000 [17], and -2002 [10]. The resultant spectra, however, are consistent with our previous ones above 10 GeV/n where the atmospheric correction is less than 3%.

5.2 Force Field Approximation

In the Force Field approximation [28], cosmic-ray spectra at various solar activities are described by introducing the interstellar (IS) proton spectrum and one “modulation parameter” ϕ . In this model, solar wind is assumed to be spherically symmetrical and is described with a simplified diffusion coefficient and a transport equation for the propagation of cosmic-ray charged particles. The Force Field approximation predicts that the cosmic-ray particle

of charge Z loses an energy of $Z\phi$, as if the particle decelerated in the static field with potential of ϕ . Although the model is too simple to describe real dynamic activity of the solar wind, it has been generally used for the analysis of cosmic-ray spectra subject to solar modulation. The model is convenient to describe the basic feature of modulated cosmic-ray spectra and to indicate a degree of the solar activity.

The proton spectra obtained under this approximation are given in Fig. 8 in comparison with our measured data. The IS proton spectrum was assumed to be described with $A\beta^{P_1}R^{-P_2}$, where, as usual, β is the velocity of the particle divided by speed of light, R is the rigidity, and A , P_1 and P_2 are the fitting parameters. The parameter ϕ for BESS-1998 was estimated to be ~ 600 MV by Myers *et al.* [29]. Other curves and values of ϕ given in Fig. 8 were obtained by fitting the measured spectra using the common IS proton spectrum. The Force Field approximation fits relatively well to the spectra measured in 1997, 1998 and 1999, which are in the positive phase of the Sun's magnetic field polarity. However, small discrepancies can be seen in 2000 and 2002, which are in the negative phase. According to recent works [30,31], the drift pattern of charged particles coming into the heliosphere varies with the sign of the polarity of heliospheric magnetic field. This feature cannot be treated in the Force Field approximation. Furthermore, the amount of energy loss depends on the observed particle energy, especially for negative polarity phase [31]. The small discrepancy seen in 2000 and 2002 may come from an inadequacy of the assumption of the model that the energy loss is independent of energy. We need further improvement in the models before we can consistently and accurately use them to estimate the shape of the interstellar spectrum.

6 Conclusion

Low energy cosmic-ray proton and helium spectra have been measured in the kinetic energy range $0.215 - 21.5$ GeV/n with the BESS balloon flights in northern Canada during a period of solar minimum, 1997, through post-maximum, 2002. The proton spectra at TOA in the five flight experiments were obtained after correction of the atmospheric proton fluxes measured in 1999 and 2000. The correction was further improved by using the pure atmospheric proton flux measured in BESS-2001 at Ft. Sumner, where the geomagnetic cut-off energy is 3.4 GeV. The helium spectra at TOA were obtained in the same way. The overall uncertainties of the spectra are 12% for protons and 18% for helium nuclei including statistical and systematic errors.

Assuming an interstellar (IS) proton spectrum and the modulation parameter ϕ of about 600 MV, the Force Field approximation can reproduce the measured spectra obtained from the BESS-1998 experiment, which are in the positive

phase of the Sun's magnetic field polarity. Further corrections or model improvements, however, would be required to reproduce the spectra during the negative polarity phase. The low energy cosmic-ray proton and helium spectra and the solar modulation effects have been much better understood based on the measurements with the BESS spectrometer in the solar minimum through post-maximum period. Those precisely measured data are important not only to study the effect of solar modulation but also to make a precise analysis of the cosmic phenomena observed at different solar activities.

Acknowledgements

We thank the NASA/GSFC/WFF Balloon office and the NSBF for the balloon expedition, and KEK and ISAS for various support. We are indebted to S.Yanagita and S.Miyake of Ibaraki University for their kindest cooperation of theoretical interpretations. This work was supported in Japan by Grant-in-Aid for Scientific Research, MEXT and by Heiwa Nakajima Foundation and JSPS in Japan, and by NASA in the USA. Analysis was performed using the computing facilities at ICEPP, the University of Tokyo.

References

- [1] P. Papini, *et al.*, Nuovo Cimento 19C (1996) 367.
- [2] S. Orito, in: Proceedings of ASTROMAG Workshop, KEK Report KEK87-19 (1987) 111.
- [3] A. Yamamoto, *et al.*, IEEE Trans. Magn. 24 (1988) 1421.
- [4] A. Yamamoto, *et al.*, Adv. Space Res. 14 (1994) 75.
- [5] Y. Ajima, *et al.*, Nucl. Instrum. Methods A 443 (2000) 71.
- [6] Y. Shikaze, *et al.*, Nucl. Instrum. Methods A 455 (2000) 596.
- [7] Y. Asaoka, *et al.*, Nucl. Instrum. Methods A 416 (1998) 236.
- [8] T. Sanuki, *et al.*, Astrophys. J. 545 (2000) 1135.
- [9] K. Abe, *et al.*, Phys. Lett. B 564 (2003) 8.
- [10] S. Haino, *et al.*, Phys. Lett. B 594 (2004) 35.
- [11] M. Motoki, *et al.*, Astropart. Phys. 19 (2003) 113.
- [12] T. Sanuki, *et al.*, Phys. Lett. B 577 (2003) 10.

- [13] K. Yoshimura, *et al.*, Phys. Rev. Lett. 75 (1995) 3792; A. Moiseev, *et al.*, Astrophys. J. 474 (1997) 479.
- [14] H. Matsunaga, *et al.*, Phys. Rev. Lett. 81 (1998) 4052.
- [15] S. Orito, *et al.*, Phys. Rev. Lett. 84 (2000) 1078.
- [16] T. Maeno, *et al.*, Astropart. Phys. 16 (2001) 121.
- [17] Y. Asaoka, *et al.*, Phys. Rev. Lett. 88 (2002) 051101.
- [18] M. Sasaki, *et al.*, Nucl. Phys. B (Proc. Suppl.) 113 (2002) 202.
- [19] V. Karimaki, Comput. Phys. Commun. 69 (1992) 133.
- [20] S. Haino, *et al.*, Nucl. Instrum. Methods A 518 (2004) 167.
- [21] Y. Asaoka, *et al.*, Nucl. Instrum. Methods A 489 (2001) 170.
- [22] <http://odysseus.uchicago.edu/NeutronMonitor/>: University of Chicago, “National Science Foundation Grant ATM-9613963”.
- [23] R. Brun, *et al.*, GEANT-Detector Description and Simulation Tool, CERN Program Library, Long Write up W5013.
- [24] M. Honda, *et al.*, Phys. Rev. D70 (2004) 043008.
- [25] E.S. Seo, *et al.*, Proceedings of 25th International Cosmic-Ray Conference, Durban, 3 (1997) 337.
- [26] J.J. Engelmann, *et al.*, Astron. Astrophys. 233 (1990) 96.
- [27] J.D. Sullivan, Nucl. Instrum. Methods 95 (1971) 5.
- [28] L.J. Gleeson, W.I. Axford, Astrophys. J. 154 (1968) 1011.
- [29] Z.D. Myers, E.S. Seo, Adv. Space Res. 35 (2005) 151.
- [30] J.W. Bieber *et al.*, Phys. Rev. Lett. 83 (1999) 674.
- [31] S. Miyake and S. Yanagita, Proceedings of 29th International Cosmic-Ray Conference, Pune, 2 (2005) 203; astro-ph/0610777; S. Miyake and S. Yanagita, private communication.

Table 1
A summary of the BESS flights.

Year	1997	1998	1999	2000	2001	2002
Location	Canada	Canada	Canada	Canada	U.S.	Canada
	Lynn Lake	Lynn Lake	Lynn Lake	Lynn Lake	Ft.Sumner	Lynn Lake
Cut-off Rigidity [GV]	0.4	0.4	0.4	0.4	4.2	0.4
Launching date	27th July	29th July	11th Aug.	10th Aug.	24th Sept.	7th Aug.
Float time [hr]	20.5	22.0	34.5	44.5	14.3*	16.5
Observation time [hr] (during ascent)	18.3	20.0	31.3	32.5	11.6	13.9
Atmos. Depth [g/cm ²]	5.0	5.5	4.3	4.3	4.5–28	4.6
Reference	[16]	[8]	[17]	[17]	[9]	[10]

* Including 11.8 hours of slow descent period

Energy range (GeV nucleon $^{-1}$)	Flux \pm Δ Flux _{sta} \pm Δ Flux _{sys} (m $^{-2}$ sr $^{-1}$ s $^{-1}$ GeV $^{-1}$ nucleon)				
	Name of BESS flights [observed year]				
	BESS-1997 [1997]	BESS-1998 [1998]	BESS-1999 [1999]	BESS-2000 [2000]	BESS-2002 [2002]
0.215– 0.251	1.83 \pm 0.03 \pm 0.13 \times 10 ³	1.22 \pm 0.02 \pm 0.09 \times 10 ³	9.88 \pm 0.20 \pm 0.76 \times 10 ²	1.69 \pm 0.04 \pm 0.18 \times 10 ²	2.22 \pm 0.05 \pm 0.17 \times 10 ²
0.251– 0.293	1.91 \pm 0.02 \pm 0.13 \times 10 ³	1.29 \pm 0.02 \pm 0.09 \times 10 ³	1.04 \pm 0.02 \pm 0.07 \times 10 ³	1.92 \pm 0.04 \pm 0.18 \times 10 ²	2.55 \pm 0.05 \pm 0.17 \times 10 ²
0.293– 0.342	1.92 \pm 0.02 \pm 0.12 \times 10 ³	1.35 \pm 0.02 \pm 0.09 \times 10 ³	1.12 \pm 0.02 \pm 0.07 \times 10 ³	2.06 \pm 0.04 \pm 0.17 \times 10 ²	2.81 \pm 0.05 \pm 0.17 \times 10 ²
0.342– 0.398	1.92 \pm 0.02 \pm 0.12 \times 10 ³	1.35 \pm 0.02 \pm 0.09 \times 10 ³	1.10 \pm 0.02 \pm 0.07 \times 10 ³	2.13 \pm 0.04 \pm 0.17 \times 10 ²	3.04 \pm 0.05 \pm 0.16 \times 10 ²
0.398– 0.464	1.84 \pm 0.02 \pm 0.11 \times 10 ³	1.33 \pm 0.02 \pm 0.08 \times 10 ³	1.09 \pm 0.02 \pm 0.07 \times 10 ³	2.32 \pm 0.04 \pm 0.17 \times 10 ²	3.21 \pm 0.05 \pm 0.16 \times 10 ²
0.464– 0.541	1.75 \pm 0.02 \pm 0.10 \times 10 ³	1.27 \pm 0.02 \pm 0.08 \times 10 ³	1.05 \pm 0.01 \pm 0.06 \times 10 ³	2.33 \pm 0.04 \pm 0.16 \times 10 ²	3.28 \pm 0.04 \pm 0.15 \times 10 ²
0.541– 0.631	1.66 \pm 0.02 \pm 0.09 \times 10 ³	1.24 \pm 0.01 \pm 0.07 \times 10 ³	9.85 \pm 0.13 \pm 0.57 \times 10 ²	2.43 \pm 0.04 \pm 0.16 \times 10 ²	3.51 \pm 0.04 \pm 0.14 \times 10 ²
0.631– 0.736	1.49 \pm 0.01 \pm 0.08 \times 10 ³	1.16 \pm 0.01 \pm 0.07 \times 10 ³	9.33 \pm 0.12 \pm 0.52 \times 10 ²	2.46 \pm 0.04 \pm 0.16 \times 10 ²	3.52 \pm 0.04 \pm 0.13 \times 10 ²
0.736– 0.858	1.37 \pm 0.01 \pm 0.07 \times 10 ³	1.07 \pm 0.01 \pm 0.06 \times 10 ³	8.57 \pm 0.10 \pm 0.47 \times 10 ²	2.48 \pm 0.03 \pm 0.15 \times 10 ²	3.46 \pm 0.04 \pm 0.12 \times 10 ²
0.858– 1.000	1.20 \pm 0.01 \pm 0.06 \times 10 ³	9.79 \pm 0.10 \pm 0.52 \times 10 ²	8.32 \pm 0.10 \pm 0.44 \times 10 ²	2.49 \pm 0.03 \pm 0.14 \times 10 ²	3.37 \pm 0.03 \pm 0.11 \times 10 ²
1.00– 1.17	1.07 \pm 0.01 \pm 0.06 \times 10 ³	8.67 \pm 0.09 \pm 0.46 \times 10 ²	7.24 \pm 0.08 \pm 0.38 \times 10 ²	2.39 \pm 0.03 \pm 0.13 \times 10 ²	3.28 \pm 0.03 \pm 0.11 \times 10 ²
1.17– 1.36	8.93 \pm 0.08 \pm 0.46 \times 10 ²	7.54 \pm 0.08 \pm 0.40 \times 10 ²	6.60 \pm 0.08 \pm 0.35 \times 10 ²	2.34 \pm 0.03 \pm 0.13 \times 10 ²	3.05 \pm 0.03 \pm 0.10 \times 10 ²
1.36– 1.58	7.49 \pm 0.07 \pm 0.38 \times 10 ²	6.45 \pm 0.07 \pm 0.35 \times 10 ²	5.58 \pm 0.06 \pm 0.30 \times 10 ²	2.12 \pm 0.02 \pm 0.12 \times 10 ²	2.87 \pm 0.03 \pm 0.09 \times 10 ²
1.58– 1.85	6.09 \pm 0.06 \pm 0.31 \times 10 ²	5.44 \pm 0.06 \pm 0.29 \times 10 ²	4.91 \pm 0.06 \pm 0.26 \times 10 ²	1.98 \pm 0.02 \pm 0.11 \times 10 ²	2.64 \pm 0.02 \pm 0.08 \times 10 ²
1.85– 2.15	5.01 \pm 0.05 \pm 0.25 \times 10 ²	4.47 \pm 0.05 \pm 0.24 \times 10 ²	3.93 \pm 0.05 \pm 0.21 \times 10 ²	1.77 \pm 0.02 \pm 0.10 \times 10 ²	2.36 \pm 0.02 \pm 0.07 \times 10 ²
2.15– 2.51	4.03 \pm 0.04 \pm 0.20 \times 10 ²	3.62 \pm 0.04 \pm 0.20 \times 10 ²	3.11 \pm 0.04 \pm 0.17 \times 10 ²	1.55 \pm 0.02 \pm 0.09 \times 10 ²	2.05 \pm 0.02 \pm 0.06 \times 10 ²
2.51– 2.93	3.14 \pm 0.03 \pm 0.16 \times 10 ²	2.90 \pm 0.03 \pm 0.16 \times 10 ²	2.61 \pm 0.03 \pm 0.15 \times 10 ²	1.34 \pm 0.01 \pm 0.08 \times 10 ²	1.72 \pm 0.01 \pm 0.05 \times 10 ²
2.93– 3.42	2.39 \pm 0.03 \pm 0.12 \times 10 ²	2.24 \pm 0.03 \pm 0.13 \times 10 ²	1.98 \pm 0.03 \pm 0.11 \times 10 ²	1.14 \pm 0.01 \pm 0.07 \times 10 ²	1.43 \pm 0.01 \pm 0.04 \times 10 ²
3.42– 3.98	1.83 \pm 0.02 \pm 0.09 \times 10 ²	1.71 \pm 0.02 \pm 0.10 \times 10 ²	1.52 \pm 0.02 \pm 0.09 \times 10 ²	9.55 \pm 0.11 \pm 0.55 \times 10	1.17 \pm 0.01 \pm 0.03 \times 10 ²
3.98– 4.64	1.39 \pm 0.02 \pm 0.07 \times 10 ²	1.27 \pm 0.02 \pm 0.07 \times 10 ²	1.15 \pm 0.02 \pm 0.07 \times 10 ²	7.75 \pm 0.09 \pm 0.45 \times 10	9.34 \pm 0.09 \pm 0.27 \times 10
4.64– 5.41	1.00 \pm 0.01 \pm 0.05 \times 10 ²	9.95 \pm 0.15 \pm 0.58 \times 10	9.28 \pm 0.15 \pm 0.54 \times 10	6.24 \pm 0.07 \pm 0.37 \times 10	7.30 \pm 0.07 \pm 0.21 \times 10
5.41– 6.31	7.54 \pm 0.11 \pm 0.37 \times 10	7.08 \pm 0.12 \pm 0.42 \times 10	6.68 \pm 0.12 \pm 0.39 \times 10	4.97 \pm 0.06 \pm 0.29 \times 10	5.59 \pm 0.06 \pm 0.16 \times 10
6.31– 7.36	5.33 \pm 0.13 \pm 0.26 \times 10	5.01 \pm 0.02 \pm 0.30 \times 10	4.82 \pm 0.03 \pm 0.29 \times 10	3.74 \pm 0.02 \pm 0.22 \times 10	4.30 \pm 0.03 \pm 0.12 \times 10
7.36– 8.58	3.65 \pm 0.10 \pm 0.18 \times 10	3.45 \pm 0.01 \pm 0.21 \times 10	3.34 \pm 0.02 \pm 0.20 \times 10	2.70 \pm 0.01 \pm 0.16 \times 10	3.11 \pm 0.04 \pm 0.09 \times 10
8.58– 10.0	2.73 \pm 0.08 \pm 0.13 \times 10	2.41 \pm 0.01 \pm 0.15 \times 10	2.43 \pm 0.02 \pm 0.15 \times 10	2.04 \pm 0.01 \pm 0.12 \times 10	2.22 \pm 0.03 \pm 0.06 \times 10
10.0– 11.7	1.86 \pm 0.06 \pm 0.09 \times 10	1.65 \pm 0.01 \pm 0.10 \times 10	1.60 \pm 0.01 \pm 0.10 \times 10	1.42 \pm 0.01 \pm 0.09 \times 10	1.55 \pm 0.01 \pm 0.05 \times 10
11.7– 13.6	1.25 \pm 0.05 \pm 0.06 \times 10	1.20 \pm 0.01 \pm 0.07 \times 10	1.16 \pm 0.01 \pm 0.07 \times 10	1.06 \pm 0.01 \pm 0.06 \times 10	1.09 \pm 0.01 \pm 0.04 \times 10
13.6– 15.8	8.63 \pm 0.37 \pm 0.42	7.96 \pm 0.05 \pm 0.49	7.88 \pm 0.07 \pm 0.48	7.22 \pm 0.04 \pm 0.44	7.49 \pm 0.04 \pm 0.27
15.8– 18.5	5.71 \pm 0.28 \pm 0.28	5.61 \pm 0.04 \pm 0.34	5.52 \pm 0.06 \pm 0.34	5.15 \pm 0.03 \pm 0.31	5.21 \pm 0.03 \pm 0.19
18.5– 21.5	3.68 \pm 0.21 \pm 0.18	3.91 \pm 0.03 \pm 0.24	3.79 \pm 0.05 \pm 0.23	3.60 \pm 0.03 \pm 0.22	3.53 \pm 0.03 \pm 0.14

Table 2
Energy spectrum of protons at the top of the atmosphere.

Energy range (GeV nucleon $^{-1}$)	Flux \pm Δ Flux _{sta} \pm Δ Flux _{sys} (m $^{-2}$ sr $^{-1}$ s $^{-1}$ GeV $^{-1}$ nucleon)				
	Name of BESS flights [observed year]				
	BESS-1997 [1997]	BESS-1998 [1998]	BESS-1999 [1999]	BESS-2000 [2000]	BESS-2002 [2002]
0.215– 0.251	$2.83 \pm 0.08 \pm 0.16 \times 10^2$	$2.21 \pm 0.07 \pm 0.12 \times 10^2$	$1.78 \pm 0.06 \pm 0.10 \times 10^2$	$4.78 \pm 0.34 \pm 0.27 \times 10$	$7.66 \pm 0.37 \pm 0.55 \times 10$
0.251– 0.293	$2.85 \pm 0.07 \pm 0.15 \times 10^2$	$2.27 \pm 0.07 \pm 0.12 \times 10^2$	$1.85 \pm 0.06 \pm 0.10 \times 10^2$	$5.41 \pm 0.34 \pm 0.30 \times 10$	$8.31 \pm 0.35 \pm 0.59 \times 10$
0.293– 0.342	$2.90 \pm 0.07 \pm 0.15 \times 10^2$	$2.29 \pm 0.06 \pm 0.12 \times 10^2$	$1.90 \pm 0.06 \pm 0.10 \times 10^2$	$6.32 \pm 0.34 \pm 0.34 \times 10$	$8.54 \pm 0.33 \pm 0.61 \times 10$
0.342– 0.398	$2.75 \pm 0.06 \pm 0.15 \times 10^2$	$2.16 \pm 0.06 \pm 0.12 \times 10^2$	$1.89 \pm 0.05 \pm 0.10 \times 10^2$	$5.57 \pm 0.30 \pm 0.30 \times 10$	$7.55 \pm 0.29 \pm 0.54 \times 10$
0.398– 0.464	$2.39 \pm 0.05 \pm 0.13 \times 10^2$	$2.18 \pm 0.05 \pm 0.12 \times 10^2$	$1.70 \pm 0.05 \pm 0.09 \times 10^2$	$6.02 \pm 0.29 \pm 0.32 \times 10$	$8.31 \pm 0.28 \pm 0.59 \times 10$
0.464– 0.541	$2.21 \pm 0.05 \pm 0.12 \times 10^2$	$1.95 \pm 0.05 \pm 0.10 \times 10^2$	$1.55 \pm 0.04 \pm 0.08 \times 10^2$	$6.30 \pm 0.28 \pm 0.34 \times 10$	$8.44 \pm 0.26 \pm 0.60 \times 10$
0.541– 0.631	$2.05 \pm 0.04 \pm 0.11 \times 10^2$	$1.70 \pm 0.04 \pm 0.09 \times 10^2$	$1.48 \pm 0.04 \pm 0.08 \times 10^2$	$5.87 \pm 0.25 \pm 0.32 \times 10$	$8.01 \pm 0.24 \pm 0.57 \times 10$
0.631– 0.736	$1.72 \pm 0.04 \pm 0.09 \times 10^2$	$1.53 \pm 0.04 \pm 0.08 \times 10^2$	$1.27 \pm 0.03 \pm 0.07 \times 10^2$	$5.52 \pm 0.23 \pm 0.30 \times 10$	$7.23 \pm 0.21 \pm 0.51 \times 10$
0.736– 0.858	$1.38 \pm 0.03 \pm 0.07 \times 10^2$	$1.27 \pm 0.03 \pm 0.07 \times 10^2$	$1.15 \pm 0.03 \pm 0.06 \times 10^2$	$5.08 \pm 0.20 \pm 0.27 \times 10$	$6.56 \pm 0.19 \pm 0.47 \times 10$
0.858– 1.000	$1.23 \pm 0.03 \pm 0.07 \times 10^2$	$1.09 \pm 0.03 \pm 0.06 \times 10^2$	$9.83 \pm 0.25 \pm 0.53 \times 10$	$4.97 \pm 0.19 \pm 0.27 \times 10$	$6.16 \pm 0.17 \pm 0.44 \times 10$
1.00– 1.17	$9.36 \pm 0.22 \pm 0.51 \times 10$	$8.60 \pm 0.22 \pm 0.47 \times 10$	$8.16 \pm 0.21 \pm 0.44 \times 10$	$4.34 \pm 0.16 \pm 0.24 \times 10$	$5.32 \pm 0.15 \pm 0.38 \times 10$
1.17– 1.36	$7.74 \pm 0.18 \pm 0.43 \times 10$	$7.47 \pm 0.19 \pm 0.41 \times 10$	$6.21 \pm 0.17 \pm 0.34 \times 10$	$3.80 \pm 0.14 \pm 0.21 \times 10$	$4.86 \pm 0.13 \pm 0.34 \times 10$
1.36– 1.58	$6.23 \pm 0.15 \pm 0.36 \times 10$	$5.57 \pm 0.15 \pm 0.31 \times 10$	$5.32 \pm 0.15 \pm 0.30 \times 10$	$3.21 \pm 0.12 \pm 0.18 \times 10$	$4.09 \pm 0.11 \pm 0.29 \times 10$
1.58– 1.85	$4.66 \pm 0.12 \pm 0.27 \times 10$	$4.40 \pm 0.13 \pm 0.25 \times 10$	$4.24 \pm 0.12 \pm 0.24 \times 10$	$2.70 \pm 0.10 \pm 0.15 \times 10$	$3.25 \pm 0.09 \pm 0.23 \times 10$
1.85– 2.15	$3.73 \pm 0.10 \pm 0.22 \times 10$	$3.58 \pm 0.11 \pm 0.21 \times 10$	$3.37 \pm 0.10 \pm 0.19 \times 10$	$2.22 \pm 0.09 \pm 0.13 \times 10$	$2.65 \pm 0.08 \pm 0.19 \times 10$
2.15– 2.51	$2.93 \pm 0.08 \pm 0.18 \times 10$	$2.72 \pm 0.08 \pm 0.16 \times 10$	$2.56 \pm 0.08 \pm 0.15 \times 10$	$1.85 \pm 0.07 \pm 0.11 \times 10$	$2.19 \pm 0.07 \pm 0.16 \times 10$
2.51– 2.93	$2.17 \pm 0.07 \pm 0.14 \times 10$	$1.90 \pm 0.07 \pm 0.11 \times 10$	$1.91 \pm 0.07 \pm 0.11 \times 10$	$1.51 \pm 0.06 \pm 0.09 \times 10$	$1.83 \pm 0.06 \pm 0.13 \times 10$
2.93– 3.42	$1.63 \pm 0.05 \pm 0.11 \times 10$	$1.49 \pm 0.05 \pm 0.09 \times 10$	$1.40 \pm 0.05 \pm 0.08 \times 10$	$1.19 \pm 0.05 \pm 0.07 \times 10$	$1.38 \pm 0.04 \pm 0.10 \times 10$
3.42– 3.98	$1.17 \pm 0.04 \pm 0.08 \times 10$	$1.09 \pm 0.04 \pm 0.07 \times 10$	$9.93 \pm 0.41 \pm 0.61$	$9.55 \pm 0.42 \pm 0.59$	$9.81 \pm 0.35 \pm 0.70$
3.98– 4.64	$9.28 \pm 0.51 \pm 0.63$	$7.80 \pm 0.11 \pm 0.49$	$7.79 \pm 0.16 \pm 0.49$	$6.32 \pm 0.09 \pm 0.39$	$7.69 \pm 0.29 \pm 0.54$
4.64– 5.41	$6.44 \pm 0.39 \pm 0.45$	$5.90 \pm 0.08 \pm 0.38$	$6.10 \pm 0.12 \pm 0.39$	$4.94 \pm 0.07 \pm 0.31$	$5.72 \pm 0.23 \pm 0.41$
5.41– 6.31	$4.66 \pm 0.31 \pm 0.34$	$4.10 \pm 0.06 \pm 0.27$	$4.37 \pm 0.09 \pm 0.28$	$3.69 \pm 0.06 \pm 0.24$	$3.98 \pm 0.06 \pm 0.32$
6.31– 7.36	$2.86 \pm 0.23 \pm 0.21$	$2.99 \pm 0.05 \pm 0.20$	$2.97 \pm 0.07 \pm 0.19$	$2.70 \pm 0.04 \pm 0.18$	$2.83 \pm 0.04 \pm 0.23$
7.36– 8.58	$2.24 \pm 0.19 \pm 0.17$	$2.03 \pm 0.04 \pm 0.14$	$2.02 \pm 0.05 \pm 0.13$	$1.86 \pm 0.03 \pm 0.12$	$2.07 \pm 0.04 \pm 0.17$
8.58– 10.0	$1.43 \pm 0.14 \pm 0.11$	$1.42 \pm 0.03 \pm 0.10$	$1.43 \pm 0.04 \pm 0.10$	$1.36 \pm 0.03 \pm 0.09$	$1.48 \pm 0.03 \pm 0.12$
10.0– 11.7	$8.92 \pm 1.04 \pm 0.70 \times 10^{-1}$	$9.99 \pm 0.23 \pm 0.68 \times 10^{-1}$	$9.85 \pm 0.34 \pm 0.67 \times 10^{-1}$	$9.32 \pm 0.22 \pm 0.63 \times 10^{-1}$	$1.03 \pm 0.02 \pm 0.08$
11.7– 13.6	$8.41 \pm 0.94 \pm 0.66 \times 10^{-1}$	$6.65 \pm 0.18 \pm 0.45 \times 10^{-1}$	$6.35 \pm 0.25 \pm 0.43 \times 10^{-1}$	$6.95 \pm 0.17 \pm 0.47 \times 10^{-1}$	$6.79 \pm 0.16 \pm 0.56 \times 10^{-1}$
13.6– 15.8	$4.78 \pm 0.66 \pm 0.38 \times 10^{-1}$	$4.37 \pm 0.13 \pm 0.30 \times 10^{-1}$	$4.77 \pm 0.20 \pm 0.33 \times 10^{-1}$	$4.63 \pm 0.13 \pm 0.32 \times 10^{-1}$	$4.73 \pm 0.12 \pm 0.39 \times 10^{-1}$
15.8– 18.5	$3.26 \pm 0.50 \pm 0.26 \times 10^{-1}$	$3.08 \pm 0.10 \pm 0.21 \times 10^{-1}$	$3.02 \pm 0.15 \pm 0.21 \times 10^{-1}$	$3.06 \pm 0.10 \pm 0.21 \times 10^{-1}$	$3.28 \pm 0.10 \pm 0.27 \times 10^{-1}$
18.5– 21.5	$2.47 \pm 0.41 \pm 0.20 \times 10^{-1}$	$2.04 \pm 0.08 \pm 0.14 \times 10^{-1}$	$2.33 \pm 0.12 \pm 0.16 \times 10^{-1}$	$1.99 \pm 0.07 \pm 0.14 \times 10^{-1}$	$2.14 \pm 0.07 \pm 0.18 \times 10^{-1}$

Table 3
Energy spectrum of helium nuclei at the top of the atmosphere.

Energy range (GeV nucleon $^{-1}$)	Flux \pm Δ Flux sta \pm Δ Flux sys (m $^{-2}$ sr $^{-1}$ s $^{-1}$ GeV $^{-1}$ nucleon)					
	atmospheric depth range [mean] (g/cm 2)					
	5.25–5.79 [5.53]	5.79–6.68 [6.29]	6.68–7.66 [6.97]	7.66–8.63 [8.10]	8.63–9.70 [9.38]	9.70–11.7 [10.8]
0.185– 0.215	1.42 \pm 0.08 \pm 0.05 $\times 10^3$	1.54 \pm 0.09 \pm 0.06 $\times 10^3$	1.47 \pm 0.09 \pm 0.06 $\times 10^3$	1.42 \pm 0.08 \pm 0.05 $\times 10^3$	1.46 \pm 0.09 \pm 0.06 $\times 10^3$	1.52 \pm 0.08 \pm 0.06 $\times 10^3$
0.215– 0.251	1.38 \pm 0.07 \pm 0.05 $\times 10^3$	1.48 \pm 0.08 \pm 0.06 $\times 10^3$	1.37 \pm 0.08 \pm 0.05 $\times 10^3$	1.49 \pm 0.08 \pm 0.06 $\times 10^3$	1.62 \pm 0.09 \pm 0.06 $\times 10^3$	1.53 \pm 0.07 \pm 0.06 $\times 10^3$
0.251– 0.293	1.39 \pm 0.06 \pm 0.05 $\times 10^3$	1.33 \pm 0.07 \pm 0.05 $\times 10^3$	1.42 \pm 0.08 \pm 0.05 $\times 10^3$	1.53 \pm 0.07 \pm 0.06 $\times 10^3$	1.61 \pm 0.08 \pm 0.06 $\times 10^3$	1.58 \pm 0.07 \pm 0.06 $\times 10^3$
0.293– 0.341	1.38 \pm 0.06 \pm 0.05 $\times 10^3$	1.37 \pm 0.07 \pm 0.05 $\times 10^3$	1.37 \pm 0.07 \pm 0.05 $\times 10^3$	1.31 \pm 0.06 \pm 0.05 $\times 10^3$	1.54 \pm 0.07 \pm 0.06 $\times 10^3$	1.43 \pm 0.06 \pm 0.05 $\times 10^3$
0.341– 0.398	1.31 \pm 0.05 \pm 0.05 $\times 10^3$	1.23 \pm 0.06 \pm 0.05 $\times 10^3$	1.25 \pm 0.06 \pm 0.05 $\times 10^3$	1.27 \pm 0.06 \pm 0.05 $\times 10^3$	1.27 \pm 0.06 \pm 0.05 $\times 10^3$	1.35 \pm 0.06 \pm 0.05 $\times 10^3$
0.398– 0.464	1.22 \pm 0.05 \pm 0.05 $\times 10^3$	1.23 \pm 0.06 \pm 0.05 $\times 10^3$	1.20 \pm 0.06 \pm 0.05 $\times 10^3$	1.26 \pm 0.06 \pm 0.05 $\times 10^3$	1.21 \pm 0.06 \pm 0.05 $\times 10^3$	1.22 \pm 0.05 \pm 0.05 $\times 10^3$
0.464– 0.541	1.07 \pm 0.05 \pm 0.04 $\times 10^3$	1.11 \pm 0.05 \pm 0.04 $\times 10^3$	1.11 \pm 0.05 \pm 0.04 $\times 10^3$	9.85 \pm 0.47 \pm 0.38 $\times 10^2$	1.16 \pm 0.05 \pm 0.04 $\times 10^3$	1.07 \pm 0.05 \pm 0.04 $\times 10^3$
0.541– 0.631	1.07 \pm 0.05 \pm 0.04 $\times 10^3$	1.15 \pm 0.05 \pm 0.04 $\times 10^3$	1.06 \pm 0.05 \pm 0.04 $\times 10^3$	1.12 \pm 0.05 \pm 0.04 $\times 10^3$	1.10 \pm 0.05 \pm 0.04 $\times 10^3$	1.05 \pm 0.05 \pm 0.04 $\times 10^3$
0.631– 0.736	9.95 \pm 0.46 \pm 0.38 $\times 10^2$	1.00 \pm 0.05 \pm 0.04 $\times 10^3$	9.30 \pm 0.52 \pm 0.36 $\times 10^2$	1.04 \pm 0.05 \pm 0.04 $\times 10^3$	1.06 \pm 0.05 \pm 0.04 $\times 10^3$	1.06 \pm 0.05 \pm 0.04 $\times 10^3$
0.736– 0.858	8.99 \pm 0.47 \pm 0.34 $\times 10^2$	9.22 \pm 0.53 \pm 0.35 $\times 10^2$	8.68 \pm 0.54 \pm 0.33 $\times 10^2$	8.86 \pm 0.51 \pm 0.34 $\times 10^2$	8.81 \pm 0.54 \pm 0.34 $\times 10^2$	1.02 \pm 0.05 \pm 0.04 $\times 10^3$
0.858– 1.000	7.32 \pm 0.50 \pm 0.28 $\times 10^2$	7.52 \pm 0.56 \pm 0.29 $\times 10^2$	8.12 \pm 0.61 \pm 0.31 $\times 10^2$	8.85 \pm 0.59 \pm 0.34 $\times 10^2$	9.23 \pm 0.64 \pm 0.35 $\times 10^2$	6.89 \pm 0.48 \pm 0.26 $\times 10^2$
1.00– 1.17	8.14 \pm 1.21 \pm 0.31 $\times 10^2$	9.64 \pm 1.47 \pm 0.37 $\times 10^2$	7.43 \pm 1.36 \pm 0.29 $\times 10^2$	7.56 \pm 1.26 \pm 0.29 $\times 10^2$	8.96 \pm 1.45 \pm 0.34 $\times 10^2$	7.36 \pm 1.15 \pm 0.28 $\times 10^2$
1.17– 1.36	6.54 \pm 1.01 \pm 0.26 $\times 10^2$	5.60 \pm 1.04 \pm 0.22 $\times 10^2$	4.90 \pm 1.02 \pm 0.19 $\times 10^2$	5.42 \pm 0.99 \pm 0.21 $\times 10^2$	6.09 \pm 1.11 \pm 0.24 $\times 10^2$	6.64 \pm 1.01 \pm 0.26 $\times 10^2$
1.36– 1.58	4.64 \pm 0.78 \pm 0.19 $\times 10^2$	5.59 \pm 0.96 \pm 0.22 $\times 10^2$	5.44 \pm 0.99 \pm 0.22 $\times 10^2$	6.31 \pm 0.99 \pm 0.25 $\times 10^2$	4.15 \pm 0.85 \pm 0.17 $\times 10^2$	5.79 \pm 0.87 \pm 0.23 $\times 10^2$
1.58– 1.85	3.99 \pm 0.67 \pm 0.16 $\times 10^2$	6.35 \pm 0.95 \pm 0.26 $\times 10^2$	5.61 \pm 0.94 \pm 0.23 $\times 10^2$	3.70 \pm 0.70 \pm 0.15 $\times 10^2$	4.30 \pm 0.80 \pm 0.18 $\times 10^2$	4.52 \pm 0.71 \pm 0.18 $\times 10^2$
1.85– 2.15	3.85 \pm 0.62 \pm 0.16 $\times 10^2$	3.42 \pm 0.65 \pm 0.14 $\times 10^2$	4.46 \pm 0.78 \pm 0.19 $\times 10^2$	3.78 \pm 0.66 \pm 0.16 $\times 10^2$	4.37 \pm 0.75 \pm 0.18 $\times 10^2$	2.74 \pm 0.52 \pm 0.11 $\times 10^2$
2.15– 2.51	3.22 \pm 0.52 \pm 0.14 $\times 10^2$	3.05 \pm 0.57 \pm 0.13 $\times 10^2$	3.13 \pm 0.60 \pm 0.13 $\times 10^2$	2.75 \pm 0.52 \pm 0.12 $\times 10^2$	2.43 \pm 0.52 \pm 0.10 $\times 10^2$	2.52 \pm 0.46 \pm 0.11 $\times 10^2$
2.51– 2.93	2.75 \pm 0.45 \pm 0.12 $\times 10^2$	2.15 \pm 0.44 \pm 0.09 $\times 10^2$	2.28 \pm 0.47 \pm 0.10 $\times 10^2$	2.35 \pm 0.44 \pm 0.10 $\times 10^2$	2.45 \pm 0.48 \pm 0.11 $\times 10^2$	2.73 \pm 0.44 \pm 0.12 $\times 10^2$
2.93– 3.41	1.63 \pm 0.32 \pm 0.07 $\times 10^2$	2.26 \pm 0.42 \pm 0.10 $\times 10^2$	1.72 \pm 0.38 \pm 0.08 $\times 10^2$	2.69 \pm 0.44 \pm 0.12 $\times 10^2$	1.31 \pm 0.33 \pm 0.06 $\times 10^2$	1.81 \pm 0.34 \pm 0.08 $\times 10^2$
3.41– 3.98	1.78 \pm 0.31 \pm 0.08 $\times 10^2$	2.01 \pm 0.37 \pm 0.09 $\times 10^2$	1.55 \pm 0.34 \pm 0.07 $\times 10^2$	1.88 \pm 0.34 \pm 0.09 $\times 10^2$	1.41 \pm 0.31 \pm 0.06 $\times 10^2$	1.18 \pm 0.25 \pm 0.05 $\times 10^2$
3.98– 4.64	1.63 \pm 0.27 \pm 0.08 $\times 10^2$	1.09 \pm 0.25 \pm 0.05 $\times 10^2$	8.27 \pm 2.29 \pm 0.38 $\times 10$	1.40 \pm 0.28 \pm 0.06 $\times 10^2$	9.69 \pm 2.42 \pm 0.45 $\times 10$	1.29 \pm 0.24 \pm 0.06 $\times 10^2$
4.64– 5.41	9.13 \pm 1.90 \pm 0.43 $\times 10$	1.03 \pm 0.23 \pm 0.05 $\times 10^2$	6.52 \pm 1.88 \pm 0.31 $\times 10$	8.29 \pm 1.95 \pm 0.39 $\times 10$	1.03 \pm 0.23 \pm 0.05 $\times 10^2$	6.30 \pm 1.58 \pm 0.30 $\times 10$
5.41– 6.31	7.87 \pm 1.64 \pm 0.38 $\times 10$	4.66 \pm 1.41 \pm 0.22 $\times 10$	6.55 \pm 1.75 \pm 0.32 $\times 10$	5.56 \pm 1.49 \pm 0.27 $\times 10$	4.90 \pm 1.48 \pm 0.24 $\times 10$	6.11 \pm 1.44 \pm 0.29 $\times 10$
6.31– 7.36	4.56 \pm 0.24 \pm 0.22 $\times 10$	4.22 \pm 0.25 \pm 0.21 $\times 10$	3.78 \pm 0.25 \pm 0.19 $\times 10$	4.46 \pm 0.25 \pm 0.22 $\times 10$	4.50 \pm 0.27 \pm 0.22 $\times 10$	4.81 \pm 0.24 \pm 0.24 $\times 10$
7.36– 8.58	3.09 \pm 0.17 \pm 0.15 $\times 10$	3.11 \pm 0.19 \pm 0.15 $\times 10$	3.13 \pm 0.20 \pm 0.16 $\times 10$	3.33 \pm 0.19 \pm 0.17 $\times 10$	2.99 \pm 0.19 \pm 0.15 $\times 10$	2.96 \pm 0.17 \pm 0.15 $\times 10$
8.58– 10.0	2.03 \pm 0.13 \pm 0.10 $\times 10$	2.59 \pm 0.16 \pm 0.13 $\times 10$	2.03 \pm 0.15 \pm 0.10 $\times 10$	2.01 \pm 0.14 \pm 0.10 $\times 10$	2.06 \pm 0.15 \pm 0.11 $\times 10$	2.11 \pm 0.13 \pm 0.11 $\times 10$
10.0– 11.7	1.62 \pm 0.11 \pm 0.08 $\times 10$	1.61 \pm 0.12 \pm 0.08 $\times 10$	1.36 \pm 0.12 \pm 0.07 $\times 10$	1.41 \pm 0.11 \pm 0.07 $\times 10$	1.45 \pm 0.12 \pm 0.07 $\times 10$	1.56 \pm 0.11 \pm 0.08 $\times 10$
11.7– 13.6	1.15 \pm 0.08 \pm 0.06 $\times 10$	1.27 \pm 0.10 \pm 0.07 $\times 10$	1.11 \pm 0.10 \pm 0.06 $\times 10$	9.43 \pm 0.81 \pm 0.49	1.11 \pm 0.09 \pm 0.06 $\times 10$	9.96 \pm 0.77 \pm 0.51
13.6– 15.8	8.05 \pm 0.64 \pm 0.42	7.36 \pm 0.68 \pm 0.38	7.17 \pm 0.70 \pm 0.37	8.12 \pm 0.69 \pm 0.42	6.89 \pm 0.67 \pm 0.36	6.79 \pm 0.58 \pm 0.35
15.8– 18.5	4.71 \pm 0.45 \pm 0.24	4.56 \pm 0.49 \pm 0.23	3.98 \pm 0.48 \pm 0.21	4.67 \pm 0.48 \pm 0.24	5.07 \pm 0.53 \pm 0.26	4.71 \pm 0.45 \pm 0.24
18.5– 21.5	2.65 \pm 0.31 \pm 0.14	2.97 \pm 0.37 \pm 0.15	3.03 \pm 0.39 \pm 0.16	3.20 \pm 0.37 \pm 0.17	3.45 \pm 0.40 \pm 0.18	3.06 \pm 0.33 \pm 0.16

Table 4
Energy spectrum of protons at the small atmospheric depths measured in BESS-1999 (1).

Energy range (GeV nucleon ⁻¹)	Flux \pm Δ Flux _{sta} \pm Δ Flux _{sys} (m ⁻² sr ⁻¹ s ⁻¹ GeV ⁻¹ nucleon)					
	atmospheric depth range [mean] (g/cm ²)					
	11.7–14.4 [12.8]	14.4–17.7 [16.2]	17.7–20.7 [19.1]	20.7–24.9 [22.5]	24.9–30.5 [28.0]	30.5–37.2 [33.7]
0.185– 0.215	1.69 \pm 0.09 \pm 0.06 $\times 10^3$	1.84 \pm 0.09 \pm 0.07 $\times 10^3$	1.87 \pm 0.10 \pm 0.07 $\times 10^3$	2.11 \pm 0.09 \pm 0.08 $\times 10^3$	2.33 \pm 0.09 \pm 0.09 $\times 10^3$	2.24 \pm 0.10 \pm 0.08 $\times 10^3$
0.215– 0.251	1.64 \pm 0.08 \pm 0.06 $\times 10^3$	1.77 \pm 0.08 \pm 0.07 $\times 10^3$	1.79 \pm 0.09 \pm 0.07 $\times 10^3$	1.82 \pm 0.08 \pm 0.07 $\times 10^3$	2.01 \pm 0.08 \pm 0.08 $\times 10^3$	2.01 \pm 0.09 \pm 0.08 $\times 10^3$
0.251– 0.293	1.55 \pm 0.07 \pm 0.06 $\times 10^3$	1.70 \pm 0.08 \pm 0.06 $\times 10^3$	1.85 \pm 0.09 \pm 0.07 $\times 10^3$	1.78 \pm 0.07 \pm 0.07 $\times 10^3$	1.96 \pm 0.07 \pm 0.07 $\times 10^3$	2.07 \pm 0.08 \pm 0.08 $\times 10^3$
0.293– 0.341	1.38 \pm 0.06 \pm 0.05 $\times 10^3$	1.58 \pm 0.07 \pm 0.06 $\times 10^3$	1.60 \pm 0.07 \pm 0.06 $\times 10^3$	1.66 \pm 0.06 \pm 0.06 $\times 10^3$	1.76 \pm 0.06 \pm 0.07 $\times 10^3$	1.89 \pm 0.07 \pm 0.07 $\times 10^3$
0.341– 0.398	1.35 \pm 0.06 \pm 0.05 $\times 10^3$	1.43 \pm 0.06 \pm 0.05 $\times 10^3$	1.33 \pm 0.06 \pm 0.05 $\times 10^3$	1.51 \pm 0.06 \pm 0.06 $\times 10^3$	1.46 \pm 0.05 \pm 0.06 $\times 10^3$	1.49 \pm 0.06 \pm 0.06 $\times 10^3$
0.398– 0.464	1.21 \pm 0.05 \pm 0.05 $\times 10^3$	1.32 \pm 0.06 \pm 0.05 $\times 10^3$	1.27 \pm 0.06 \pm 0.05 $\times 10^3$	1.30 \pm 0.05 \pm 0.05 $\times 10^3$	1.26 \pm 0.05 \pm 0.05 $\times 10^3$	1.31 \pm 0.06 \pm 0.05 $\times 10^3$
0.464– 0.541	1.19 \pm 0.05 \pm 0.05 $\times 10^3$	1.21 \pm 0.05 \pm 0.05 $\times 10^3$	1.11 \pm 0.05 \pm 0.04 $\times 10^3$	1.16 \pm 0.05 \pm 0.04 $\times 10^3$	1.21 \pm 0.05 \pm 0.05 $\times 10^3$	1.20 \pm 0.05 \pm 0.05 $\times 10^3$
0.541– 0.631	1.08 \pm 0.05 \pm 0.04 $\times 10^3$	1.01 \pm 0.05 \pm 0.04 $\times 10^3$	1.09 \pm 0.05 \pm 0.04 $\times 10^3$	1.08 \pm 0.05 \pm 0.04 $\times 10^3$	1.12 \pm 0.04 \pm 0.04 $\times 10^3$	1.13 \pm 0.05 \pm 0.04 $\times 10^3$
0.631– 0.736	9.73 \pm 0.47 \pm 0.37 $\times 10^2$	1.06 \pm 0.05 \pm 0.04 $\times 10^3$	1.01 \pm 0.05 \pm 0.04 $\times 10^3$	9.74 \pm 0.45 \pm 0.37 $\times 10^2$	9.93 \pm 0.43 \pm 0.38 $\times 10^2$	1.07 \pm 0.05 \pm 0.04 $\times 10^3$
0.736– 0.858	9.50 \pm 0.51 \pm 0.36 $\times 10^2$	9.07 \pm 0.51 \pm 0.35 $\times 10^2$	9.48 \pm 0.56 \pm 0.36 $\times 10^2$	9.13 \pm 0.47 \pm 0.35 $\times 10^2$	1.03 \pm 0.05 \pm 0.04 $\times 10^3$	8.56 \pm 0.50 \pm 0.33 $\times 10^2$
0.858– 1.000	8.49 \pm 0.56 \pm 0.32 $\times 10^2$	8.26 \pm 0.57 \pm 0.31 $\times 10^2$	8.30 \pm 0.61 \pm 0.32 $\times 10^2$	8.85 \pm 0.54 \pm 0.34 $\times 10^2$	8.64 \pm 0.51 \pm 0.33 $\times 10^2$	7.92 \pm 0.56 \pm 0.30 $\times 10^2$
1.00– 1.17	7.00 \pm 1.17 \pm 0.27 $\times 10^2$	7.07 \pm 1.21 \pm 0.27 $\times 10^2$	5.57 \pm 1.16 \pm 0.21 $\times 10^2$	5.62 \pm 0.99 \pm 0.22 $\times 10^2$	7.18 \pm 1.07 \pm 0.28 $\times 10^2$	5.83 \pm 1.10 \pm 0.22 $\times 10^2$
1.17– 1.36	5.53 \pm 0.96 \pm 0.22 $\times 10^2$	6.98 \pm 1.12 \pm 0.27 $\times 10^2$	8.75 \pm 1.35 \pm 0.34 $\times 10^2$	5.29 \pm 0.89 \pm 0.21 $\times 10^2$	6.46 \pm 0.94 \pm 0.25 $\times 10^2$	5.73 \pm 1.01 \pm 0.22 $\times 10^2$
1.36– 1.58	4.28 \pm 0.78 \pm 0.17 $\times 10^2$	3.81 \pm 0.76 \pm 0.15 $\times 10^2$	4.26 \pm 0.87 \pm 0.17 $\times 10^2$	6.30 \pm 0.90 \pm 0.25 $\times 10^2$	4.91 \pm 0.76 \pm 0.20 $\times 10^2$	5.49 \pm 0.92 \pm 0.22 $\times 10^2$
1.58– 1.85	5.39 \pm 0.81 \pm 0.22 $\times 10^2$	4.97 \pm 0.81 \pm 0.20 $\times 10^2$	4.42 \pm 0.82 \pm 0.18 $\times 10^2$	3.65 \pm 0.63 \pm 0.15 $\times 10^2$	5.32 \pm 0.73 \pm 0.22 $\times 10^2$	3.80 \pm 0.71 \pm 0.16 $\times 10^2$
1.85– 2.15	4.24 \pm 0.67 \pm 0.18 $\times 10^2$	3.85 \pm 0.66 \pm 0.16 $\times 10^2$	2.77 \pm 0.60 \pm 0.12 $\times 10^2$	3.54 \pm 0.58 \pm 0.15 $\times 10^2$	3.31 \pm 0.54 \pm 0.14 $\times 10^2$	3.40 \pm 0.62 \pm 0.14 $\times 10^2$
2.15– 2.51	3.01 \pm 0.52 \pm 0.13 $\times 10^2$	3.12 \pm 0.55 \pm 0.13 $\times 10^2$	2.38 \pm 0.52 \pm 0.10 $\times 10^2$	2.47 \pm 0.45 \pm 0.10 $\times 10^2$	3.07 \pm 0.48 \pm 0.13 $\times 10^2$	3.32 \pm 0.57 \pm 0.14 $\times 10^2$
2.51– 2.93	3.03 \pm 0.49 \pm 0.13 $\times 10^2$	2.66 \pm 0.47 \pm 0.12 $\times 10^2$	3.29 \pm 0.56 \pm 0.14 $\times 10^2$	1.82 \pm 0.36 \pm 0.08 $\times 10^2$	1.79 \pm 0.34 \pm 0.08 $\times 10^2$	2.50 \pm 0.46 \pm 0.11 $\times 10^2$
2.93– 3.41	2.50 \pm 0.41 \pm 0.11 $\times 10^2$	1.66 \pm 0.35 \pm 0.07 $\times 10^2$	1.68 \pm 0.38 \pm 0.10 $\times 10^2$	2.31 \pm 0.38 \pm 0.10 $\times 10^2$	1.94 \pm 0.33 \pm 0.09 $\times 10^2$	1.66 \pm 0.35 \pm 0.07 $\times 10^2$
3.41– 3.98	1.45 \pm 0.29 \pm 0.07 $\times 10^2$	1.24 \pm 0.28 \pm 0.06 $\times 10^2$	1.95 \pm 0.38 \pm 0.09 $\times 10^2$	1.10 \pm 0.24 \pm 0.05 $\times 10^2$	1.43 \pm 0.26 \pm 0.06 $\times 10^2$	1.49 \pm 0.30 \pm 0.07 $\times 10^2$
3.98– 4.64	1.20 \pm 0.24 \pm 0.06 $\times 10^2$	1.01 \pm 0.23 \pm 0.05 $\times 10^2$	9.95 \pm 2.49 \pm 0.46 $\times 10$	1.49 \pm 0.26 \pm 0.07 $\times 10^2$	1.11 \pm 0.21 \pm 0.05 $\times 10^2$	1.28 \pm 0.26 \pm 0.06 $\times 10^2$
4.64– 5.41	8.11 \pm 1.86 \pm 0.38 $\times 10$	5.93 \pm 1.65 \pm 0.28 $\times 10$	1.06 \pm 0.24 \pm 0.05 $\times 10^2$	9.24 \pm 1.89 \pm 0.44 $\times 10$	7.35 \pm 1.60 \pm 0.35 $\times 10$	9.60 \pm 2.09 \pm 0.45 $\times 10$
5.41– 6.31	5.52 \pm 1.42 \pm 0.27 $\times 10$	6.68 \pm 1.62 \pm 0.32 $\times 10$	7.32 \pm 1.83 \pm 0.35 $\times 10$	7.96 \pm 1.63 \pm 0.38 $\times 10$	3.92 \pm 1.09 \pm 0.19 $\times 10$	4.72 \pm 1.36 \pm 0.23 $\times 10$
6.31– 7.36	3.90 \pm 0.23 \pm 0.19 $\times 10$	4.12 \pm 0.24 \pm 0.20 $\times 10$	3.81 \pm 0.25 \pm 0.19 $\times 10$	4.16 \pm 0.22 \pm 0.20 $\times 10$	3.80 \pm 0.20 \pm 0.19 $\times 10$	3.84 \pm 0.23 \pm 0.19 $\times 10$
7.36– 8.58	2.73 \pm 0.17 \pm 0.14 $\times 10$	2.83 \pm 0.18 \pm 0.14 $\times 10$	2.73 \pm 0.19 \pm 0.14 $\times 10$	2.79 \pm 0.16 \pm 0.14 $\times 10$	2.94 \pm 0.16 \pm 0.15 $\times 10$	2.63 \pm 0.17 \pm 0.13 $\times 10$
8.58– 10.0	2.28 \pm 0.14 \pm 0.12 $\times 10$	1.95 \pm 0.13 \pm 0.10 $\times 10$	2.04 \pm 0.15 \pm 0.10 $\times 10$	1.90 \pm 0.12 \pm 0.10 $\times 10$	1.78 \pm 0.11 \pm 0.09 $\times 10$	1.69 \pm 0.12 \pm 0.09 $\times 10$
10.0– 11.7	1.39 \pm 0.10 \pm 0.07 $\times 10$	1.60 \pm 0.11 \pm 0.08 $\times 10$	1.38 \pm 0.11 \pm 0.07 $\times 10$	1.42 \pm 0.10 \pm 0.07 $\times 10$	1.42 \pm 0.09 \pm 0.07 $\times 10$	1.17 \pm 0.10 \pm 0.06 $\times 10$
11.7– 13.6	1.11 \pm 0.08 \pm 0.06 $\times 10$	1.11 \pm 0.09 \pm 0.06 $\times 10$	1.02 \pm 0.09 \pm 0.05 $\times 10$	9.39 \pm 0.74 \pm 0.48	1.03 \pm 0.07 \pm 0.05 $\times 10$	8.53 \pm 0.77 \pm 0.44
13.6– 15.8	6.01 \pm 0.57 \pm 0.31	6.77 \pm 0.63 \pm 0.35	6.40 \pm 0.66 \pm 0.33	6.49 \pm 0.56 \pm 0.34	5.68 \pm 0.50 \pm 0.29	5.85 \pm 0.58 \pm 0.30
15.8– 18.5	4.00 \pm 0.43 \pm 0.21	4.33 \pm 0.46 \pm 0.22	3.72 \pm 0.46 \pm 0.19	4.48 \pm 0.43 \pm 0.23	4.53 \pm 0.41 \pm 0.23	4.68 \pm 0.48 \pm 0.24
18.5– 21.5	3.04 \pm 0.34 \pm 0.16	3.04 \pm 0.36 \pm 0.16	3.49 \pm 0.41 \pm 0.18	3.03 \pm 0.33 \pm 0.16	2.69 \pm 0.29 \pm 0.14	3.13 \pm 0.36 \pm 0.16

Table 5
Energy spectrum of protons at the small atmospheric depths measured in BESS-1999 (2).

Energy range (GeV nucleon ⁻¹)	Flux \pm Δ Flux _{sta} \pm Δ Flux _{sys} (m ⁻² sr ⁻¹ s ⁻¹ GeV ⁻¹ nucleon)					
	atmospheric depth range [mean] (g/cm ²)					
	4.00–5.00 [4.31]	5.00–6.00 [5.44]	6.00–7.00 [6.41]	7.00–8.00 [7.49]	8.00–9.00 [8.36]	9.00–10.0 [9.53]
0.185– 0.215	$3.63 \pm 0.12 \pm 0.14 \times 10^2$	$3.40 \pm 0.31 \pm 0.13 \times 10^2$	$4.48 \pm 0.50 \pm 0.17 \times 10^2$	$4.67 \pm 0.52 \pm 0.18 \times 10^2$	$4.31 \pm 0.51 \pm 0.16 \times 10^2$	$6.61 \pm 0.63 \pm 0.25 \times 10^2$
0.215– 0.251	$3.37 \pm 0.11 \pm 0.13 \times 10^2$	$3.49 \pm 0.28 \pm 0.13 \times 10^2$	$2.91 \pm 0.37 \pm 0.11 \times 10^2$	$4.74 \pm 0.47 \pm 0.18 \times 10^2$	$3.75 \pm 0.44 \pm 0.14 \times 10^2$	$5.25 \pm 0.51 \pm 0.20 \times 10^2$
0.251– 0.293	$3.41 \pm 0.10 \pm 0.13 \times 10^2$	$3.44 \pm 0.26 \pm 0.13 \times 10^2$	$3.56 \pm 0.37 \pm 0.14 \times 10^2$	$4.34 \pm 0.42 \pm 0.17 \times 10^2$	$4.47 \pm 0.44 \pm 0.17 \times 10^2$	$4.45 \pm 0.43 \pm 0.17 \times 10^2$
0.293– 0.341	$3.36 \pm 0.09 \pm 0.13 \times 10^2$	$3.71 \pm 0.25 \pm 0.14 \times 10^2$	$3.46 \pm 0.34 \pm 0.13 \times 10^2$	$3.48 \pm 0.35 \pm 0.13 \times 10^2$	$4.47 \pm 0.41 \pm 0.17 \times 10^2$	$4.22 \pm 0.39 \pm 0.16 \times 10^2$
0.341– 0.398	$3.31 \pm 0.09 \pm 0.13 \times 10^2$	$3.37 \pm 0.23 \pm 0.13 \times 10^2$	$4.01 \pm 0.35 \pm 0.15 \times 10^2$	$3.07 \pm 0.31 \pm 0.12 \times 10^2$	$4.09 \pm 0.37 \pm 0.16 \times 10^2$	$3.99 \pm 0.36 \pm 0.15 \times 10^2$
0.398– 0.464	$3.00 \pm 0.08 \pm 0.11 \times 10^2$	$3.56 \pm 0.22 \pm 0.14 \times 10^2$	$3.71 \pm 0.32 \pm 0.14 \times 10^2$	$3.72 \pm 0.33 \pm 0.14 \times 10^2$	$2.86 \pm 0.30 \pm 0.11 \times 10^2$	$3.76 \pm 0.34 \pm 0.14 \times 10^2$
0.464– 0.541	$3.05 \pm 0.08 \pm 0.12 \times 10^2$	$3.02 \pm 0.20 \pm 0.12 \times 10^2$	$3.44 \pm 0.31 \pm 0.13 \times 10^2$	$3.30 \pm 0.30 \pm 0.13 \times 10^2$	$3.57 \pm 0.33 \pm 0.14 \times 10^2$	$3.05 \pm 0.30 \pm 0.12 \times 10^2$
0.541– 0.631	$2.86 \pm 0.08 \pm 0.11 \times 10^2$	$3.06 \pm 0.20 \pm 0.12 \times 10^2$	$3.38 \pm 0.31 \pm 0.13 \times 10^2$	$3.44 \pm 0.31 \pm 0.13 \times 10^2$	$3.02 \pm 0.30 \pm 0.12 \times 10^2$	$2.95 \pm 0.29 \pm 0.11 \times 10^2$
0.631– 0.736	$2.90 \pm 0.08 \pm 0.11 \times 10^2$	$3.33 \pm 0.22 \pm 0.13 \times 10^2$	$2.63 \pm 0.28 \pm 0.10 \times 10^2$	$3.09 \pm 0.30 \pm 0.12 \times 10^2$	$3.15 \pm 0.32 \pm 0.12 \times 10^2$	$2.98 \pm 0.31 \pm 0.11 \times 10^2$
0.736– 0.858	$2.88 \pm 0.09 \pm 0.11 \times 10^2$	$2.64 \pm 0.21 \pm 0.10 \times 10^2$	$3.10 \pm 0.33 \pm 0.12 \times 10^2$	$3.25 \pm 0.34 \pm 0.12 \times 10^2$	$3.59 \pm 0.37 \pm 0.14 \times 10^2$	$3.48 \pm 0.36 \pm 0.13 \times 10^2$
0.858– 1.000	$2.58 \pm 0.10 \pm 0.10 \times 10^2$	$2.96 \pm 0.27 \pm 0.11 \times 10^2$	$2.74 \pm 0.36 \pm 0.10 \times 10^2$	$3.31 \pm 0.40 \pm 0.13 \times 10^2$	$2.69 \pm 0.38 \pm 0.10 \times 10^2$	$2.24 \pm 0.34 \pm 0.09 \times 10^2$
1.00– 1.17	$2.66 \pm 0.16 \pm 0.10 \times 10^2$	$2.99 \pm 0.43 \pm 0.11 \times 10^2$	$2.21 \pm 0.52 \pm 0.08 \times 10^2$	$2.12 \pm 0.51 \pm 0.08 \times 10^2$	$2.70 \pm 0.60 \pm 0.10 \times 10^2$	$3.00 \pm 0.63 \pm 0.12 \times 10^2$
1.17– 1.36	$2.66 \pm 0.15 \pm 0.10 \times 10^2$	$2.66 \pm 0.37 \pm 0.10 \times 10^2$	$2.84 \pm 0.55 \pm 0.11 \times 10^2$	$2.78 \pm 0.54 \pm 0.11 \times 10^2$	$1.96 \pm 0.48 \pm 0.08 \times 10^2$	$2.57 \pm 0.54 \pm 0.10 \times 10^2$
1.36– 1.58	$2.01 \pm 0.12 \pm 0.08 \times 10^2$	$2.35 \pm 0.33 \pm 0.09 \times 10^2$	$2.54 \pm 0.48 \pm 0.10 \times 10^2$	$3.14 \pm 0.54 \pm 0.13 \times 10^2$	$2.79 \pm 0.53 \pm 0.11 \times 10^2$	$2.99 \pm 0.54 \pm 0.12 \times 10^2$
1.58– 1.85	$2.02 \pm 0.11 \pm 0.08 \times 10^2$	$1.93 \pm 0.27 \pm 0.08 \times 10^2$	$1.79 \pm 0.37 \pm 0.07 \times 10^2$	$1.18 \pm 0.31 \pm 0.05 \times 10^2$	$1.88 \pm 0.40 \pm 0.08 \times 10^2$	$2.56 \pm 0.46 \pm 0.10 \times 10^2$
1.85– 2.15	$1.87 \pm 0.10 \pm 0.08 \times 10^2$	$2.03 \pm 0.26 \pm 0.08 \times 10^2$	$2.34 \pm 0.40 \pm 0.10 \times 10^2$	$1.22 \pm 0.29 \pm 0.05 \times 10^2$	$1.84 \pm 0.37 \pm 0.08 \times 10^2$	$1.71 \pm 0.35 \pm 0.07 \times 10^2$
2.15– 2.51	$1.83 \pm 0.09 \pm 0.08 \times 10^2$	$1.15 \pm 0.18 \pm 0.05 \times 10^2$	$1.62 \pm 0.31 \pm 0.07 \times 10^2$	$1.88 \pm 0.33 \pm 0.08 \times 10^2$	$2.03 \pm 0.36 \pm 0.09 \times 10^2$	$1.72 \pm 0.32 \pm 0.07 \times 10^2$
2.51– 2.93	$1.27 \pm 0.07 \pm 0.06 \times 10^2$	$1.43 \pm 0.19 \pm 0.06 \times 10^2$	$8.93 \pm 2.10 \pm 0.39 \times 10$	$1.56 \pm 0.28 \pm 0.07 \times 10^2$	$1.52 \pm 0.29 \pm 0.07 \times 10^2$	$1.21 \pm 0.25 \pm 0.05 \times 10^2$
2.93– 3.41	$1.16 \pm 0.06 \pm 0.05 \times 10^2$	$1.21 \pm 0.16 \pm 0.05 \times 10^2$	$7.66 \pm 1.81 \pm 0.34 \times 10$	$1.04 \pm 0.21 \pm 0.05 \times 10^2$	$1.12 \pm 0.23 \pm 0.05 \times 10^2$	$9.50 \pm 2.07 \pm 0.42 \times 10$
3.41– 3.98	$9.11 \pm 0.50 \pm 0.41 \times 10$	$9.49 \pm 1.32 \pm 0.43 \times 10$	$9.55 \pm 1.87 \pm 0.43 \times 10$	$8.95 \pm 1.83 \pm 0.41 \times 10$	$7.26 \pm 1.71 \pm 0.33 \times 10$	$1.09 \pm 0.21 \pm 0.05 \times 10^2$
3.98– 4.64	$7.43 \pm 0.42 \pm 0.34 \times 10$	$7.20 \pm 1.06 \pm 0.33 \times 10$	$9.14 \pm 1.70 \pm 0.42 \times 10$	$8.64 \pm 1.66 \pm 0.40 \times 10$	$8.65 \pm 1.73 \pm 0.40 \times 10$	$8.03 \pm 1.64 \pm 0.37 \times 10$
4.64– 5.41	$6.32 \pm 0.36 \pm 0.30 \times 10$	$6.05 \pm 0.90 \pm 0.29 \times 10$	$6.49 \pm 1.33 \pm 0.31 \times 10$	$6.05 \pm 1.29 \pm 0.29 \times 10$	$6.83 \pm 1.42 \pm 0.32 \times 10$	$4.02 \pm 1.08 \pm 0.19 \times 10$
5.41– 6.31	$4.57 \pm 0.28 \pm 0.22 \times 10$	$4.49 \pm 0.72 \pm 0.22 \times 10$	$5.10 \pm 1.09 \pm 0.24 \times 10$	$4.47 \pm 1.03 \pm 0.21 \times 10$	$5.09 \pm 1.14 \pm 0.24 \times 10$	$4.68 \pm 1.07 \pm 0.22 \times 10$
6.31– 7.36	$3.54 \pm 0.06 \pm 0.17 \times 10$	$3.67 \pm 0.17 \pm 0.18 \times 10$	$3.59 \pm 0.24 \pm 0.18 \times 10$	$3.74 \pm 0.24 \pm 0.18 \times 10$	$3.53 \pm 0.24 \pm 0.17 \times 10$	$3.43 \pm 0.24 \pm 0.17 \times 10$
7.36– 8.58	$2.59 \pm 0.05 \pm 0.13 \times 10$	$2.69 \pm 0.13 \pm 0.13 \times 10$	$2.63 \pm 0.18 \pm 0.13 \times 10$	$3.01 \pm 0.19 \pm 0.15 \times 10$	$2.38 \pm 0.18 \pm 0.12 \times 10$	$2.49 \pm 0.18 \pm 0.12 \times 10$
8.58– 10.0	$1.95 \pm 0.04 \pm 0.10 \times 10$	$2.06 \pm 0.10 \pm 0.11 \times 10$	$1.86 \pm 0.14 \pm 0.09 \times 10$	$2.05 \pm 0.15 \pm 0.10 \times 10$	$1.88 \pm 0.15 \pm 0.10 \times 10$	$2.03 \pm 0.15 \pm 0.10 \times 10$
10.0– 11.7	$1.38 \pm 0.03 \pm 0.07 \times 10$	$1.52 \pm 0.08 \pm 0.08 \times 10$	$1.30 \pm 0.11 \pm 0.07 \times 10$	$1.38 \pm 0.11 \pm 0.07 \times 10$	$1.50 \pm 0.12 \pm 0.08 \times 10$	$1.42 \pm 0.12 \pm 0.07 \times 10$
11.7– 13.6	$1.03 \pm 0.02 \pm 0.05 \times 10$	$9.22 \pm 0.60 \pm 0.48$	$9.48 \pm 0.87 \pm 0.49$	$9.95 \pm 0.89 \pm 0.51$	$9.88 \pm 0.93 \pm 0.51$	$8.98 \pm 0.87 \pm 0.46$
13.6– 15.8	$7.21 \pm 0.19 \pm 0.37$	$7.48 \pm 0.50 \pm 0.39$	$7.23 \pm 0.70 \pm 0.37$	$6.59 \pm 0.67 \pm 0.34$	$6.60 \pm 0.70 \pm 0.34$	$7.10 \pm 0.71 \pm 0.37$
15.8– 18.5	$4.72 \pm 0.14 \pm 0.24$	$4.45 \pm 0.36 \pm 0.23$	$4.91 \pm 0.53 \pm 0.25$	$4.52 \pm 0.51 \pm 0.23$	$4.12 \pm 0.51 \pm 0.21$	$4.42 \pm 0.52 \pm 0.23$
18.5– 21.5	$3.31 \pm 0.11 \pm 0.17$	$3.33 \pm 0.29 \pm 0.17$	$3.37 \pm 0.41 \pm 0.17$	$2.67 \pm 0.37 \pm 0.14$	$2.50 \pm 0.37 \pm 0.13$	$2.90 \pm 0.39 \pm 0.15$

Table 6
Energy spectrum of protons at the small atmospheric depths measured in BESS-2000 (1).

Table 7
Energy spectrum of protons at the small atmospheric depths measured in BESS-
2000 (2).

Energy range (GeV nucleon ⁻¹)	Flux \pm Δ Flux _{sta} \pm Δ Flux _{sys} (m ⁻² sr ⁻¹ s ⁻¹ GeV ⁻¹ nucleon)					
	atmospheric depth range [mean] (g/cm ²)					
	10.0–12.0 [11.1]	14.0–17.0 [16.1]	17.0–20.0 [18.6]	20.0–24.0 [21.7]	24.0–30.0 [27.2]	30.0–37.0 [33.6]
0.185– 0.215	5.54 \pm 0.51 \pm 0.21 $\times 10^2$	6.29 \pm 0.56 \pm 0.24 $\times 10^2$	7.16 \pm 0.63 \pm 0.27 $\times 10^2$	6.95 \pm 0.52 \pm 0.26 $\times 10^2$	7.89 \pm 0.55 \pm 0.30 $\times 10^2$	9.11 \pm 0.59 \pm 0.34 $\times 10^2$
0.215– 0.251	5.43 \pm 0.46 \pm 0.21 $\times 10^2$	6.69 \pm 0.53 \pm 0.25 $\times 10^2$	6.64 \pm 0.55 \pm 0.25 $\times 10^2$	7.70 \pm 0.50 \pm 0.29 $\times 10^2$	7.86 \pm 0.50 \pm 0.30 $\times 10^2$	8.97 \pm 0.53 \pm 0.34 $\times 10^2$
0.251– 0.293	4.97 \pm 0.41 \pm 0.19 $\times 10^2$	5.14 \pm 0.43 \pm 0.20 $\times 10^2$	7.18 \pm 0.53 \pm 0.27 $\times 10^2$	6.52 \pm 0.42 \pm 0.25 $\times 10^2$	7.92 \pm 0.46 \pm 0.30 $\times 10^2$	7.57 \pm 0.45 \pm 0.29 $\times 10^2$
0.293– 0.341	5.10 \pm 0.39 \pm 0.19 $\times 10^2$	5.18 \pm 0.40 \pm 0.20 $\times 10^2$	5.80 \pm 0.44 \pm 0.22 $\times 10^2$	5.99 \pm 0.38 \pm 0.23 $\times 10^2$	6.46 \pm 0.39 \pm 0.25 $\times 10^2$	6.67 \pm 0.39 \pm 0.25 $\times 10^2$
0.341– 0.398	4.36 \pm 0.34 \pm 0.17 $\times 10^2$	5.69 \pm 0.40 \pm 0.22 $\times 10^2$	5.07 \pm 0.39 \pm 0.19 $\times 10^2$	5.43 \pm 0.34 \pm 0.21 $\times 10^2$	5.60 \pm 0.34 \pm 0.21 $\times 10^2$	5.96 \pm 0.35 \pm 0.23 $\times 10^2$
0.398– 0.464	3.50 \pm 0.29 \pm 0.13 $\times 10^2$	4.05 \pm 0.32 \pm 0.16 $\times 10^2$	4.61 \pm 0.36 \pm 0.18 $\times 10^2$	4.70 \pm 0.30 \pm 0.18 $\times 10^2$	5.04 \pm 0.31 \pm 0.19 $\times 10^2$	5.56 \pm 0.33 \pm 0.21 $\times 10^2$
0.464– 0.541	3.99 \pm 0.30 \pm 0.15 $\times 10^2$	4.07 \pm 0.32 \pm 0.16 $\times 10^2$	4.24 \pm 0.34 \pm 0.16 $\times 10^2$	4.12 \pm 0.28 \pm 0.16 $\times 10^2$	4.61 \pm 0.29 \pm 0.18 $\times 10^2$	4.91 \pm 0.30 \pm 0.19 $\times 10^2$
0.541– 0.631	3.26 \pm 0.28 \pm 0.12 $\times 10^2$	3.76 \pm 0.31 \pm 0.14 $\times 10^2$	3.16 \pm 0.29 \pm 0.12 $\times 10^2$	4.31 \pm 0.29 \pm 0.16 $\times 10^2$	4.36 \pm 0.29 \pm 0.17 $\times 10^2$	4.85 \pm 0.30 \pm 0.18 $\times 10^2$
0.631– 0.736	3.48 \pm 0.30 \pm 0.13 $\times 10^2$	3.64 \pm 0.31 \pm 0.14 $\times 10^2$	3.66 \pm 0.33 \pm 0.14 $\times 10^2$	3.98 \pm 0.29 \pm 0.15 $\times 10^2$	3.58 \pm 0.27 \pm 0.14 $\times 10^2$	3.68 \pm 0.27 \pm 0.14 $\times 10^2$
0.736– 0.858	3.27 \pm 0.31 \pm 0.12 $\times 10^2$	3.76 \pm 0.35 \pm 0.14 $\times 10^2$	3.49 \pm 0.35 \pm 0.13 $\times 10^2$	3.46 \pm 0.29 \pm 0.13 $\times 10^2$	3.66 \pm 0.30 \pm 0.14 $\times 10^2$	3.85 \pm 0.30 \pm 0.15 $\times 10^2$
0.858– 1.000	3.02 \pm 0.35 \pm 0.11 $\times 10^2$	2.69 \pm 0.34 \pm 0.10 $\times 10^2$	2.76 \pm 0.36 \pm 0.10 $\times 10^2$	2.98 \pm 0.32 \pm 0.11 $\times 10^2$	3.51 \pm 0.34 \pm 0.13 $\times 10^2$	2.98 \pm 0.31 \pm 0.11 $\times 10^2$
1.00– 1.17	1.88 \pm 0.44 \pm 0.07 $\times 10^2$	2.67 \pm 0.54 \pm 0.10 $\times 10^2$	2.92 \pm 0.60 \pm 0.11 $\times 10^2$	2.14 \pm 0.43 \pm 0.08 $\times 10^2$	3.02 \pm 0.50 \pm 0.12 $\times 10^2$	2.69 \pm 0.47 \pm 0.10 $\times 10^2$
1.17– 1.36	2.51 \pm 0.47 \pm 0.10 $\times 10^2$	2.38 \pm 0.48 \pm 0.09 $\times 10^2$	2.92 \pm 0.55 \pm 0.11 $\times 10^2$	3.08 \pm 0.47 \pm 0.12 $\times 10^2$	2.73 \pm 0.44 \pm 0.11 $\times 10^2$	2.44 \pm 0.42 \pm 0.10 $\times 10^2$
1.36– 1.58	3.25 \pm 0.50 \pm 0.13 $\times 10^2$	2.06 \pm 0.41 \pm 0.08 $\times 10^2$	1.35 \pm 0.35 \pm 0.05 $\times 10^2$	3.16 \pm 0.45 \pm 0.13 $\times 10^2$	3.29 \pm 0.45 \pm 0.13 $\times 10^2$	2.61 \pm 0.40 \pm 0.10 $\times 10^2$
1.58– 1.85	1.59 \pm 0.32 \pm 0.07 $\times 10^2$	1.83 \pm 0.36 \pm 0.07 $\times 10^2$	2.31 \pm 0.42 \pm 0.09 $\times 10^2$	1.84 \pm 0.32 \pm 0.08 $\times 10^2$	1.70 \pm 0.30 \pm 0.07 $\times 10^2$	2.07 \pm 0.33 \pm 0.08 $\times 10^2$
1.85– 2.15	2.22 \pm 0.36 \pm 0.09 $\times 10^2$	1.64 \pm 0.31 \pm 0.07 $\times 10^2$	1.86 \pm 0.35 \pm 0.08 $\times 10^2$	1.54 \pm 0.27 \pm 0.06 $\times 10^2$	2.56 \pm 0.34 \pm 0.11 $\times 10^2$	2.29 \pm 0.32 \pm 0.10 $\times 10^2$
2.15– 2.51	1.67 \pm 0.29 \pm 0.07 $\times 10^2$	1.46 \pm 0.28 \pm 0.06 $\times 10^2$	1.03 \pm 0.24 \pm 0.04 $\times 10^2$	1.89 \pm 0.28 \pm 0.08 $\times 10^2$	1.62 \pm 0.25 \pm 0.07 $\times 10^2$	1.54 \pm 0.25 \pm 0.07 $\times 10^2$
2.51– 2.93	1.10 \pm 0.22 \pm 0.05 $\times 10^2$	1.17 \pm 0.23 \pm 0.05 $\times 10^2$	1.47 \pm 0.27 \pm 0.06 $\times 10^2$	1.11 \pm 0.20 \pm 0.05 $\times 10^2$	1.39 \pm 0.22 \pm 0.06 $\times 10^2$	1.22 \pm 0.20 \pm 0.05 $\times 10^2$
2.93– 3.41	1.49 \pm 0.23 \pm 0.07 $\times 10^2$	1.08 \pm 0.20 \pm 0.05 $\times 10^2$	6.33 \pm 1.63 \pm 0.28 $\times 10$	1.04 \pm 0.18 \pm 0.05 $\times 10^2$	9.89 \pm 1.70 \pm 0.44 $\times 10$	8.43 \pm 1.57 \pm 0.37 $\times 10$
3.41– 3.98	9.39 \pm 1.71 \pm 0.43 $\times 10$	1.06 \pm 0.19 \pm 0.05 $\times 10^2$	1.02 \pm 0.19 \pm 0.05 $\times 10^2$	1.69 \pm 0.21 \pm 0.08 $\times 10^2$	1.03 \pm 0.16 \pm 0.05 $\times 10^2$	1.00 \pm 0.16 \pm 0.05 $\times 10^2$
3.98– 4.64	6.44 \pm 1.31 \pm 0.30 $\times 10$	6.84 \pm 1.40 \pm 0.32 $\times 10$	9.37 \pm 1.71 \pm 0.43 $\times 10$	6.59 \pm 1.20 \pm 0.30 $\times 10$	6.46 \pm 1.18 \pm 0.30 $\times 10$	5.17 \pm 1.05 \pm 0.24 $\times 10$
4.64– 5.41	6.68 \pm 1.24 \pm 0.32 $\times 10$	4.90 \pm 1.09 \pm 0.23 $\times 10$	7.24 \pm 1.39 \pm 0.34 $\times 10$	5.28 \pm 1.00 \pm 0.25 $\times 10$	6.66 \pm 1.11 \pm 0.31 $\times 10$	7.21 \pm 1.15 \pm 0.34 $\times 10$
5.41– 6.31	4.14 \pm 0.90 \pm 0.20 $\times 10$	6.71 \pm 1.19 \pm 0.32 $\times 10$	3.21 \pm 0.86 \pm 0.15 $\times 10$	3.87 \pm 0.79 \pm 0.19 $\times 10$	3.48 \pm 0.74 \pm 0.17 $\times 10$	3.96 \pm 0.79 \pm 0.19 $\times 10$
6.31– 7.36	3.52 \pm 0.21 \pm 0.17 $\times 10$	3.69 \pm 0.23 \pm 0.18 $\times 10$	2.96 \pm 0.21 \pm 0.15 $\times 10$	3.60 \pm 0.20 \pm 0.18 $\times 10$	2.91 \pm 0.18 \pm 0.14 $\times 10$	3.19 \pm 0.18 \pm 0.16 $\times 10$
7.36– 8.58	2.62 \pm 0.17 \pm 0.13 $\times 10$	2.45 \pm 0.17 \pm 0.12 $\times 10$	2.37 \pm 0.17 \pm 0.12 $\times 10$	2.44 \pm 0.15 \pm 0.12 $\times 10$	2.59 \pm 0.15 \pm 0.13 $\times 10$	2.26 \pm 0.14 \pm 0.11 $\times 10$
8.58– 10.0	1.88 \pm 0.13 \pm 0.10 $\times 10$	1.82 \pm 0.13 \pm 0.09 $\times 10$	1.98 \pm 0.14 \pm 0.10 $\times 10$	1.88 \pm 0.12 \pm 0.10 $\times 10$	1.90 \pm 0.12 \pm 0.10 $\times 10$	1.60 \pm 0.11 \pm 0.08 $\times 10$
10.0– 11.7	1.59 \pm 0.11 \pm 0.08 $\times 10$	1.18 \pm 0.10 \pm 0.06 $\times 10$	1.32 \pm 0.11 \pm 0.07 $\times 10$	1.34 \pm 0.09 \pm 0.07 $\times 10$	1.22 \pm 0.09 \pm 0.06 $\times 10$	1.12 \pm 0.08 \pm 0.06 $\times 10$
11.7– 13.6	9.48 \pm 0.80 \pm 0.49	1.07 \pm 0.09 \pm 0.06 $\times 10$	9.70 \pm 0.87 \pm 0.50	8.69 \pm 0.69 \pm 0.45	8.58 \pm 0.68 \pm 0.44	8.95 \pm 0.70 \pm 0.46
13.6– 15.8	7.08 \pm 0.64 \pm 0.37	6.11 \pm 0.61 \pm 0.32	5.15 \pm 0.59 \pm 0.27	6.40 \pm 0.55 \pm 0.33	5.82 \pm 0.52 \pm 0.30	5.17 \pm 0.49 \pm 0.27
15.8– 18.5	4.68 \pm 0.48 \pm 0.24	4.81 \pm 0.50 \pm 0.25	5.27 \pm 0.55 \pm 0.27	4.23 \pm 0.41 \pm 0.22	4.42 \pm 0.42 \pm 0.23	4.97 \pm 0.44 \pm 0.26
18.5– 21.5	2.83 \pm 0.35 \pm 0.15	3.23 \pm 0.38 \pm 0.17	3.54 \pm 0.42 \pm 0.18	3.42 \pm 0.34 \pm 0.18	2.44 \pm 0.29 \pm 0.13	2.57 \pm 0.30 \pm 0.13

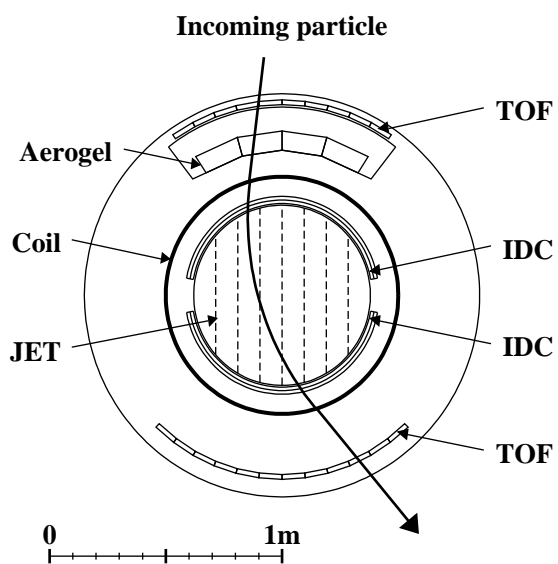


Fig. 1. Cross-sectional view of the BESS detector in its 1997 configuration.

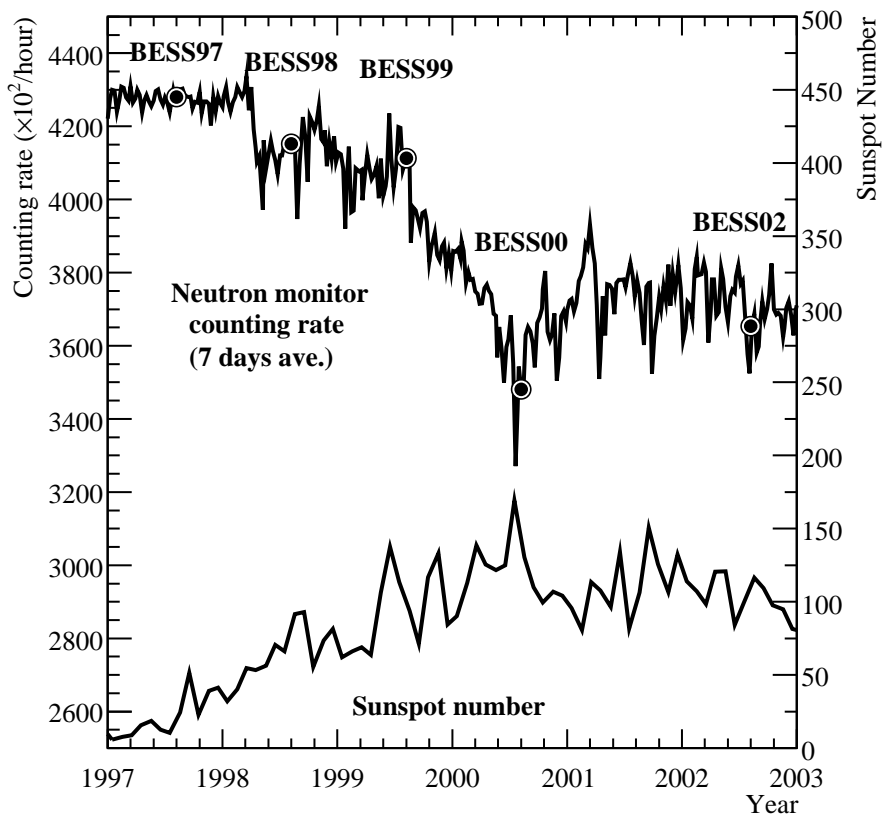


Fig. 2. Counting rate of Climax neutron monitor (7-day average) and sunspot number together with the BESS flight time [22].

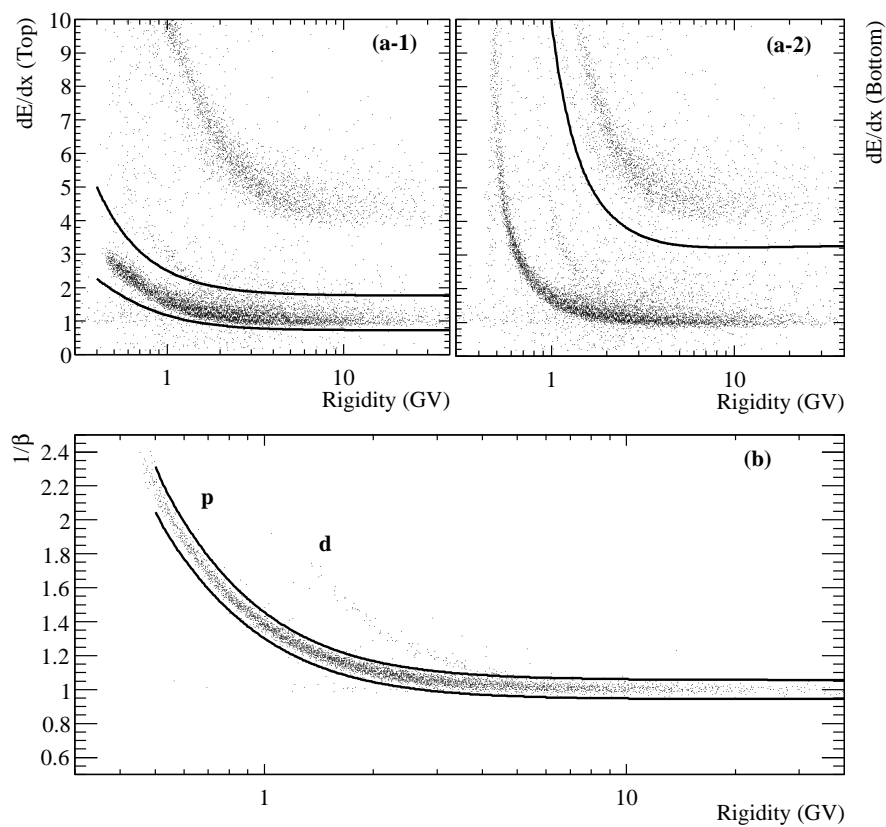


Fig. 3. Proton selection by dE/dx -band cut for the top and bottom TOF hodoscope (a-1 and a-2) and $1/\beta$ -band cut (b).

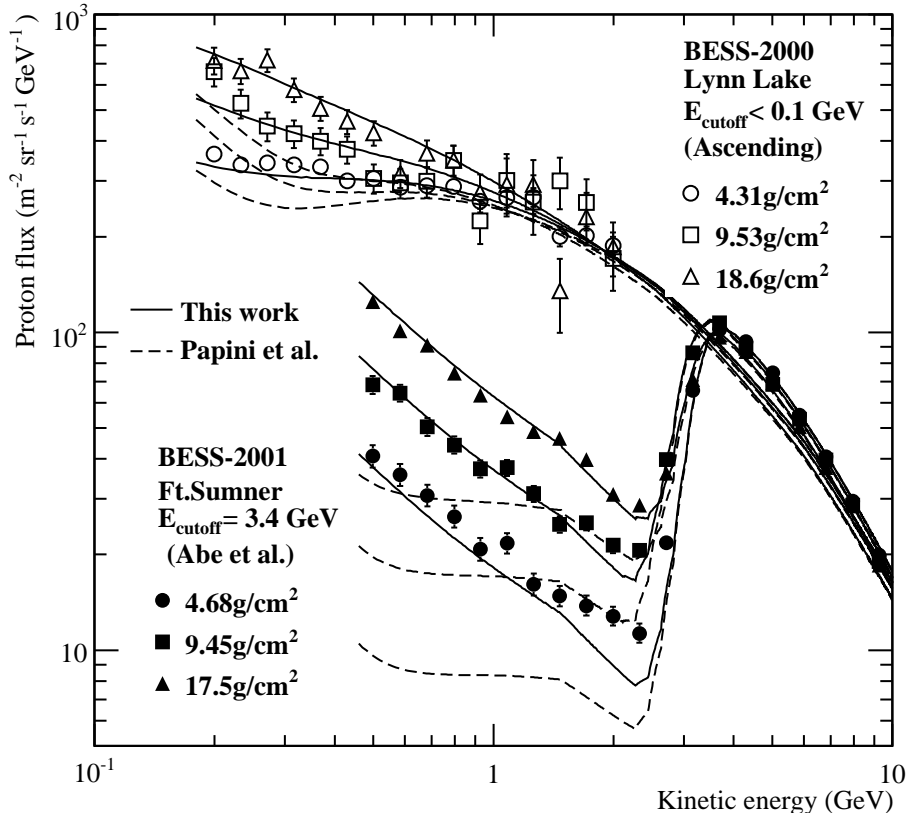


Fig. 4. Proton energy spectra at several atmospheric depths. Obtained spectra measured during the ascent in 2000 (open markers), and the descent at Ft. Sumner in 2001 [9] (closed markers) are compared with calculated spectra before (dashed lines) and after (solid lines) modification of the recoil proton production energy spectrum.

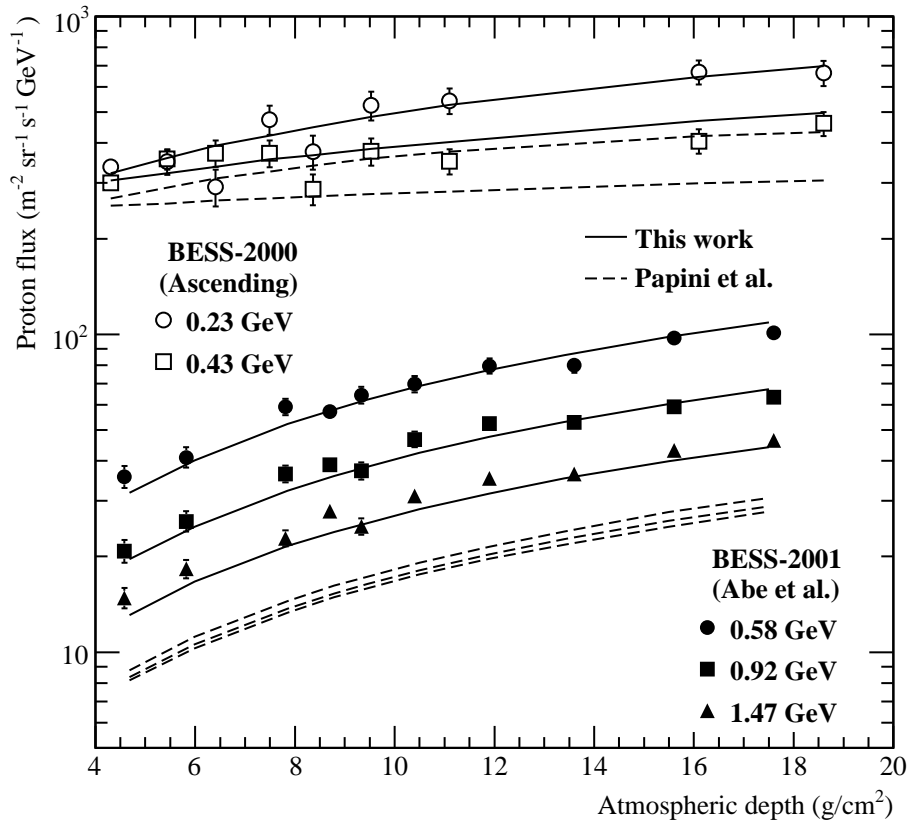


Fig. 5. Proton flux as a function of atmospheric depth. Obtained fluxes measured during the ascent in 2000 (open markers), and the descent at Ft. Sumner in 2001 (closed markers) are compared with calculated fluxes before (dashed lines) and after (solid lines) modification of the recoil proton production energy spectrum.

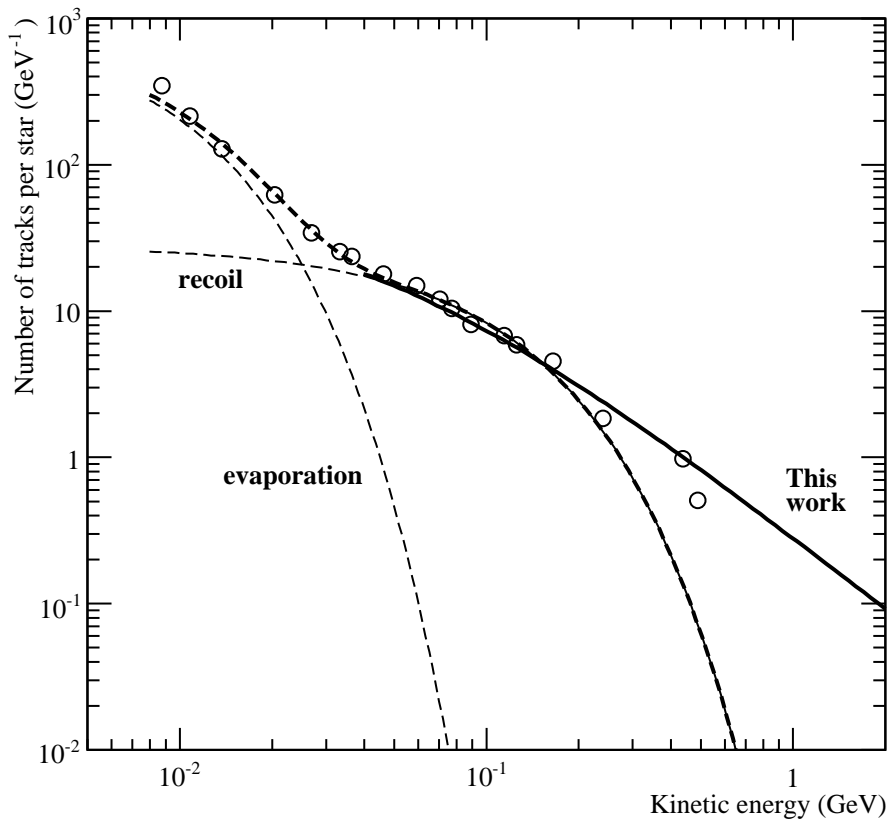


Fig. 6. The original (dashed) and modified (solid) energy spectra of secondary proton production. For the original spectrum, two dominant components of evaporation and recoil production from air nuclei are also shown. The data points are found in Ref. [1]

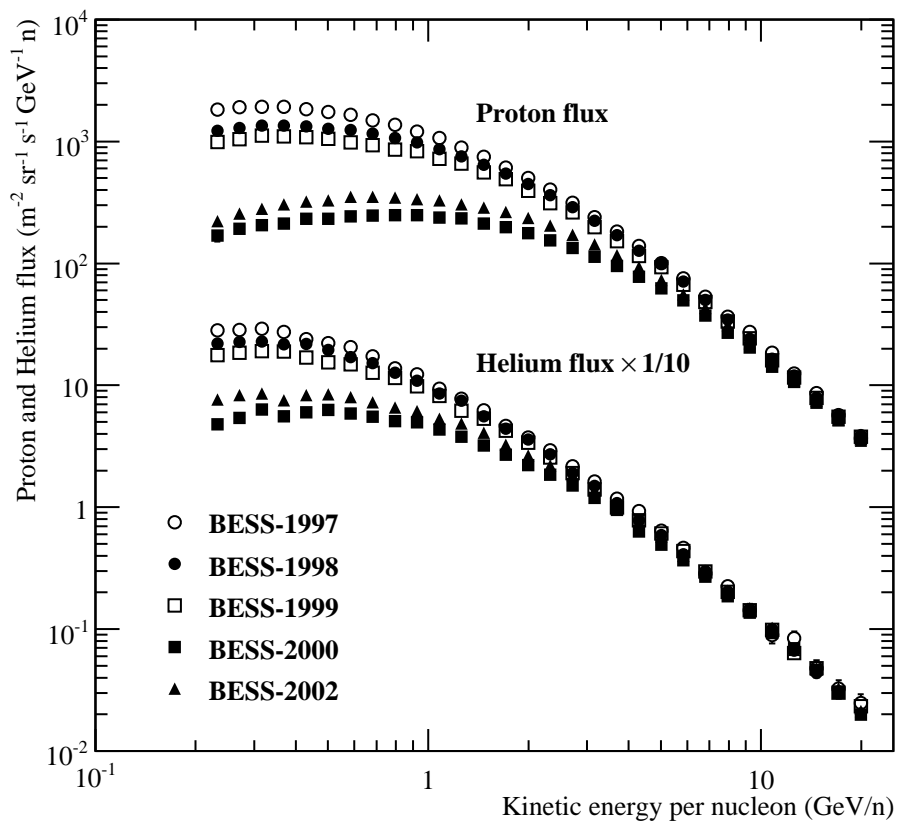


Fig. 7. Proton and helium fluxes at the top of the atmosphere from 1997 through 2002. Note that helium fluxes are plotted after being divided by a factor of 10.

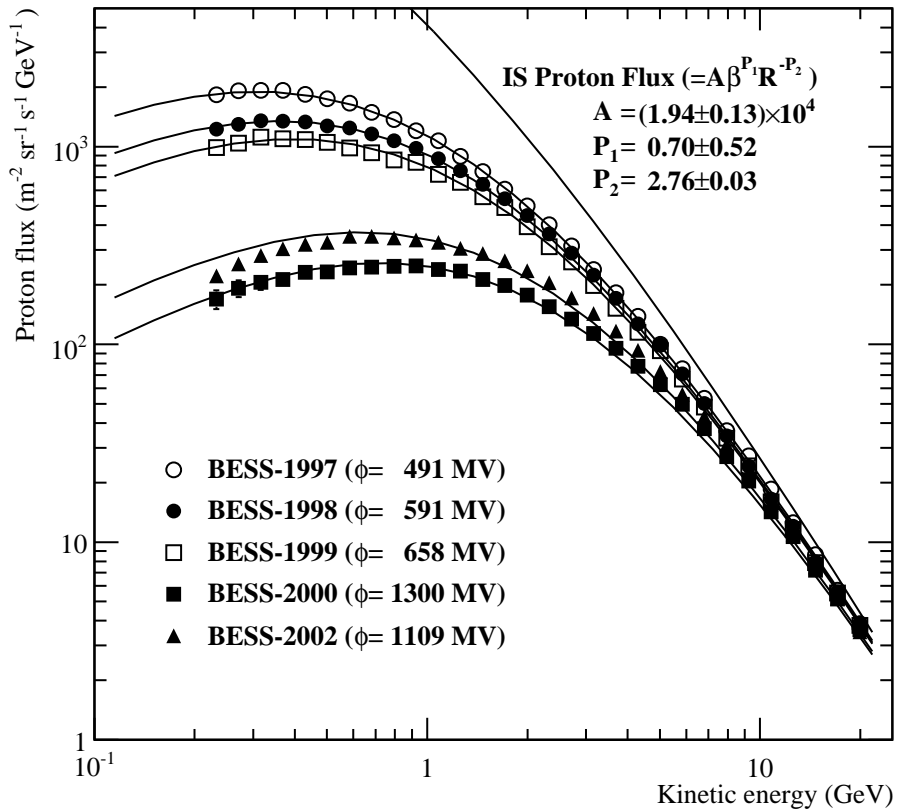


Fig. 8. Proton spectra derived under the Force Field approximation. The interstellar (IS) proton spectrum was estimated by assuming $\phi \sim 600$ MV for BESS-1998. Other curves and the value of ϕ were obtained by fitting the BESS data.